UNIVERSIDADE FEDERAL DE PERNAMBUCO
CENTRO DE TECNOLOGIA E GEOCIÊNCIAS
DEPARTAMENTO DE ELETRÔNICA E SISTEMAS
PROGRAMA DE PÓS-GRADUAÇÃO EM ENGENHARIA ELÉTRICA

JORGE ANTONIO DE ISASA ARAUJO

COPLANAR WAVEGUIDE SENSOR FOR DIMETHYL METHYLPHOSPHONATE GAS DETECTION AT MICROWAVE FREQUENCIES

Recife
2024

JORGE ANTONIO DE ISASA ARAUJO

COPLANAR WAVEGUIDE SENSOR FOR DIMETHYL METHYLPHOSPHONATE GAS DETECTION AT MICROWAVE FREQUENCIES

Thesis presented to the Postgraduate Program in Electrical Engineering at the Federal University of Pernambuco, as a partial requirement for the attainment of the title of doctor in electrical engineering.

Area of Concentration: Photonics.

Supervisor: Prof. Dr. Marcos Tavares de Melo.

Co-supervisor: Prof. Dr. Ignacio Llamas-Garro.

Recife

2024

Catalogação na fonte
Bibliotecária Margareth Malta, CRB-4 / 1198

A663c Araujo, Jorge Antonio de Isasa.
Coplanar waveguide sensor for Dimethyl Methylphosphonate gas detection at microwave frequencies / Jorge Antonio de Isasa Araujo – 2024.
78 f.: il., figs., tabs., abrev. e siglas.

Orientador: Prof. Dr. Marcos Tavares de Melo.
Coorientador: Prof. Dr. Ignacio Llamas-Garro.
Tese (Doutorado) – Universidade Federal de Pernambuco. CTG. Programa de Pós-Graduação em Engenharia Elétrica, 2024.
Inclui Referências.

1. Engenharia Elétrica. 2. Metilfosfonato de dimetilo. 3. Micro-ondas. 4. Paládio. 5. Segurança. 6. Sensor. I. Melo, Marcos Tavares de (Orientador). II. Llamas-Garro, Ignacio (Coorientador). III. Título.

UFPE

621.3 CDD (22. ed.) BCTG/2024-70

JORGE ANTONIO DE ISASA ARAUJO

COPLANAR WAVEGUIDE SENSOR FOR DIMETHYL METHYLPHOSPHONATE GAS DETECTION AT MICROWAVE FREQUENCIES

Thesis presented to the Postgraduate Program in Electrical Engineering at the Federal University of Pernambuco, Technology and Geosciences Center, as a partial requirement for the attainment of the title of Doctor in Electrical Engineering. Area of Concentration: Photonics.

Approved: 02/02/2024

THESIS COMMITTEE

_____

Prof. Dr. Marcos Tavares de Melo (Supervisor)
Universidade Federal de Pernambuco

_____

Prof. Dr. Renato Evangelista de Araujo (Internal Examiner)
Universidade Federal de Pernambuco

_____

Dr. Leonardo Morais da Silva (External Examiner)
Tribunal Regional do Trabalho da 1a Região de São Paulo

_____

Dr. Francisco Rodrigues Sabino Junior (External Examiner)
Companhia Hidrelétrica do São Francisco

_____

Prof. Dr. Zabdiel Brito-Brito (External Examiner)
Centre Tecnològic de Telecomunicacions de Catalunya

I dedicate this work to God, for being my Peace and Strength.

To my mother, Nair, to my father, Jorge, and to my brother, Manuel, for all the love, dedication, and care they have always given me.

To all my friends who have been part of this journey by my side.

ACKNOWLEDGMENTS

The acknowledgments to everyone who accompanied me on this journey would certainly make another thesis, but I begin by expressing special thanks to God for granting me the courage, strength, and good health to undertake this work and complete this extensive doctoral journey.

To my mother, Nair, for her unconditional love and her efforts in raising me and teaching me that education is the primary means of personal transformation.

To my father, Jorge, for the love and care he has given me.

To my brother, Jorge Manuel, who has been with me since birth, always supporting and motivating me.

To my relatives who have always been present and cheered for everything to go well.

To my supervisor, professor, and friend, Marcos Tavares, who always believed in me more than I believed in myself. Thank you for your advice and guidance.

To my professors Ignacio and Brito, who accompanied me during my internship at CTTC in Barcelona.

To my new grandparents, uncles, cousins, and friends whom I met in Recife and Barcelona.

To the LabMicro team: Pedro Henrique, Wilson, Francisco, Manuelle, Crislane, Marcelo, and Hawson, for always being available to contribute, with a special mention to Crislane who was directly involved in this project.

To my friends Ana, Ary, Brenno, Carol, Dannilo, Elis, Pedro, Paulo and Válbio, who have been with me since the first day of college.

To my friends Annalisa, Marc, Marco, Matthieu, and Keila, whom I had the pleasure of meeting during my exchange program in Barcelona during this doctoral period.

To the professors who served on the defense committee of this thesis and dedicated their time to reading and correcting this work.

Lastly, to everyone who contributed to this work and to my personal development.

No puc més.

ABSTRACT

This study proposes the development of a Palladium-based Coplanar Waveguide (CPW) microwave sensor for the detection of Dimethyl Methylphosphonate (DMMP) gas, considering its importance in warfare security contexts. DMMP is a chemical compound commonly used in the production of nerve agents, making it a critical target for detection in military environments. The sensor was fabricated using the spin coating and lift-off method, ensuring a uniform deposition of a thin palladium layer onto a planar substrate. The interaction between palladium and DMMP leads to changes in the dielectric properties of the sensor, which can be detected using microwave techniques. These variations were processed and analyzed to identify the presence of DMMP in the environment. The sensor underwent experimental testing in a controlled environment, where S_{21} values were measured. Specifically, DMMP was evaluated at a concentration of 400 parts per million (ppm). It was observed that the presence of DMMP caused changes in the attenuation of the S_{21} parameter, demonstrating the sensor's sensitivity to the target gas.

Keywords: dimethyl methylphosphonate; microwaves; palladium; sensor; warfare security.

RESUMO

Este trabalho propõe o desenvolvimento de um sensor CPW de micro-ondas baseado em paládio para detecção do gás Metilfosfonato de dimetilo (DMMP), considerando sua importância para a segurança em contextos de guerra. O DMMP é um composto químico frequentemente utilizado na produção de agentes nervosos, tornando-se um alvo crítico para detecção em ambientes militares. O sensor foi fabricado por meio do método de spin coating e lift off, garantindo uma deposição uniforme da camada fina de paládio sobre um substrato planar. A interação entre o paládio e o DMMP resulta em mudanças nas propriedades dielétricas do sensor, que podem ser detectadas por meio de técnicas de micro-ondas. Essas variações foram então processadas e analisadas para identificar a presença do DMMP no ambiente. O sensor foi submetido a testes experimentais em um ambiente controlado, nos quais foram medidos os valores de S_{21}. Em particular, o DMMP foi avaliado em uma concentração de 400 partes por milhão (ppm). Observou-se que a presença de DMMP causou alterações na atenuação do parâmetro S_{21}, demonstrando a sensibilidade do sensor ao gás em questão.

Palavras-chave: Metilfosfonato de dimetilo; micro-ondas; paládio; segurança; sensor.

LIST OF FIGURES

LIST OF ABBREVIATIONS AND ACRONYMS

CST	Computer Simulation Technology
CPW	Coplanar Waveguide
DFP	Diisopropyl Fluorophosphate
DIMP	Diisopropyl Methylphosphonate
DMMP	Dimethyl Methylphosphonate
FEM	Finite Element Method
ICFO	Institut de Ciències Fotòniques
INTA	Instituto Nacional de Técnica Aeroespacial
MMP	Methyl Methylphosphonate
MP	Methylphosphonate
PPB	Parts Per Billion
PPM	Parts Per Million
TE	Transverse Electric Mode
TEM	Transverse Electromagnetic Mode
TEP	Triethylphosphate
TM	Transverse Magnetic Mode

LIST OF SYMBOLS

α_c	Conductor Loss
σ_f	Electrical Conductivity
δ_s	Skin Depth
ε_f	Electrical Permittivity
ε_r	Relative Permittivity
μ_f	Magnetic Permeability
R_s	Electrical Resistivity

TABLE OF CONTENTS

1 INTRODUCTION

This chapter aims to provide a concise and objective contextualization of the subject matter covered in this thesis by offering a review of the existing literature and establishing the intended objectives. To achieve this, concepts and definitions related to the topic will be addressed and a brief analysis of previously published works.

1.1 CONTEXT

Chemical warfare agents are highly toxic and dangerous compounds, especially nerve agents such as Sarin and Soman [1]. When these gases enter the body through inhalation or skin contact, they are extremely volatile and can lead to the paralysis of neuromuscular transmissions within minutes, potentially resulting in death [2]. It is crucial to develop effective means to detect and prevent the use of these agents in enclosed environments such as buildings or public transportation systems to protect human life and ensure national security.

Following the terrorist attack in the Tokyo subway in 1995, there has been a growing need for systems to detect and monitor toxic agents, which are often colorless and odorless gases [3]. To ensure safety in laboratories, it is common to use dimethyl methylphosphonate (DMMP) as a substance to simulate the properties of these agents. DMMP has a molecular structure similar to that of Sarin and is safe to work with at lower concentrations [4].

In recent years, the need for detection and monitoring systems for toxic gases including Sarin gas and its analog DMMP has increased. For this purpose, various approaches have been developed and improved, including detection techniques based on surface acoustic wave devices [5], gas chromatography [6], and fluorometry [7].

Despite different approaches, the methods available so far have not been able to provide effective solutions for rapid and real-time detection of these nerve agents. This is largely due to the lack of portability, complexity of operation, high cost, and slow processing of existing systems [8].

Detection systems for these agents must meet the requirements of real-world applications with high sensitivity, ease of operation, and real-time responses. It is worth noting that the main form of contamination by these agents is through the air, making it more advantageous for detection systems to be more sensitive to gases than to liquids or fluids [9].

1.2 PROBLEM CHARACTERIZATION

With the technological advancements in recent years, various types of microwave-based sensors can be found in the literature that are employed in diverse applications [10]. Among them, sensors for chemical testing in liquids [11,12], detection of food and agricultural products [13,14], and measurements in industrial materials [15,16] stand out.

Recently, theoretical and practical progress has shown that sensor detection capability can be improved by adopting coplanar waveguide (CPW) configurations as microwave sensors. In this modality, both the central track and the lateral conductor are printed on the same substrate plane, thus reducing dispersion, sensitivity to interference, and minimizing possible edge effects. In this case, transmission and reflection techniques are used to identify and characterize materials [17].

When designing microwave structures as sensors for material characterization and identification, several methods can be used, including resonant and non-resonant methods. Among these methods, resonant methods present good sensitivity and precision [18]. An example of a resonant method is the resonant perturbation method, which consists of detecting changes in the resonance frequency in microwave devices when in contact with a sample [19].

These changes in the sensors' resonance frequency are induced by alterations in the electrical properties of these devices.

Among these properties, the electrical conductivity of the metal used as a sensor element stands out, as observed in [20].

This study proposes the use of a coplanar microwave sensor as an alternative for detecting the concentration of the DMMP gas in the environment. The sensor was designed with specific materials for sensing DMMP gas such as palladium and laboratory-available components. For this application, a coplanar waveguide (CPW) line-type sensor was selected.

1.3 STATE-OF-THE-ART

There are several gas sensing devices based on microwave sensors described in the scientific literature [21]-[30].

Work [21] describes the detection of ammonia gas through a waveguide-based sensor with a ground plane using cobalt phthalocyanine as the conductive metal due to its known sensitivity. The authors tested the metal as ground plane and microstrip line and observed that

the metal as microstrip line showed higher sensitivity to the concentration of ammonia gas. However, it was not possible to establish a clear pattern between the sensor responses and the exact real-time gas concentration, which was one of the goals of the work.

In another work described in [22], researchers employed a different resonator geometry using a double split-ring resonator and a conductive polymer to detect the presence of ethanol gas. A shift in the S_{21} parameter was observed in the range between 13 and 17 GHz, allowing the identification of the gas presence in the environment. Tests were performed only for a specific concentration of 100 ppm of ethanol gas, which was the initial goal of the research.

In the study described in [23], a circular resonator geometry was used to detect the presence of ammonia gas. Instead of a gas-sensitive conductive metal, a conductive film made of multiwalled carbon nanotubes was used on the circular resonator.

This idea is justified in [24], which demonstrates that carbon nanotube films and metallic oxides exhibit significant variation in their dielectric properties when in contact with gases. The proposed sensor showed S_{21} parameter shifts when ammonia gas came into contact with the structure. However, the extreme difficulty in inkjet printing these carbon nanotube films makes the system impractical and difficult to reproduce.

In [25], another metal oxide-based sensor was used, with titanium dioxide as the conductive element in a microstrip planar sensor with interdigital capacitor resonator. This sensor could detect concentrations between 100 and 500 ppm of ammonia gas and its S_{21} response showed a clear relationship with the added ammonia concentration. The sensor exhibited greater simplicity and precision in detection compared to other microwave-based ammonia gas sensors reported in the literature.

In [26], the importance of using metal oxides was also demonstrated. A microstrip patch antenna coated with a hybrid ink of reduced graphene oxide and silver was used for ammonia gas detection. The sensor was able to differentiate ammonia gas concentrations between 0 and 200 ppm in the frequency range of 5.70–5.90 GHz due to the variation of attenuation in the S_{21} parameter in dB. However, the authors highlighted that microstrip antennas have some limitations, such as narrow bandwidth and low radiation power, which may not be suitable for some applications.

A strategy to improve the sensitivity of microstrip sensors was proposed by the authors in [27], who implemented a trapezoidal spiral resonator known for its multiband characteristics. The structure was coated with a layer of titanium dioxide nanoparticles that interact with ammonia gas. Despite the attempt to make the device multiband, the system showed sensitivity

only at the frequency of 7.76 GHz where it was able to identify concentration variation between 0 and 300 ppm.

To improve the detection of gases at low concentrations, the use of CPW structure for the fabrication of planar sensors was proposed in [28]. The CPW sensor features a resonator covered by a copper oxide film, which is sensitive to acetone gas. The device was evaluated in the frequency range of 1.5-4.5 GHz, where it proved to be efficient in detecting gas concentrations in real time in the range of 0.5-5 ppm. The performance of the sensor indicates the high efficiency of CPW structures for sensing low gas concentrations.

The work [29] presented a microwave sensor with an interdigital resonator structure coated with a vapor-sensitive polymer known as PSE, designed in CPW to operate at 4 GHz. Measured results for five samples of ammonium hydroxide concentration showed that gas concentration levels could be detected by measuring changes in the transmission coefficient.

The article [30] presents a simple, economical, and wideband strategy for noninvasive sweat monitoring using a microwave sensor and cellulose filter paper as superstrate. The suggested sensor consists of filter paper on top of a coplanar transmission line capable of identifying concentrations of 0.01 mol/L (0.58 g/L) and quantities as small as 137 μL. The variation in transmission coefficient (S_{21}) between dry and wet states is used to measure the concentrations of the solutions evaluated in the frequency range of 1-6 GHz.

1.4 GOALS

The general and specific objectives are listed below.

1.4.1 Overall goal

To develop a gas sensor capable of detecting DMMP in the environment using a coplanar waveguide (CPW) structure coated with palladium.

1.4.2 Specific goals

- To computationally model the sensor using 3D electromagnetic software and simulate the variation caused by the interaction with DMMP gas;
- Fabricate and measure this device;

- Compare simulation and measurement results to verify the effectiveness of the system and discuss hypotheses.

1.5 THESIS STRUCTURE

- Chapter 1 – Introduction: In this chapter, the study theme is introduced, a brief literature review is presented, and the general and specific objectives intended for the thesis are outlined;
- Chapter 2 – Theoretical Framework: This chapter presents the definition and main characteristics of the proposed system, as well as the theoretical foundation necessary for its understanding, based on extensive reference material;
- Chapter 3 – Materials and Methodological Procedures: This chapter addresses all the steps taken to design, manufacture and measure the prototypes studied;
- Chapter 4 – Numerical and Experimental Results: analysis, comparison, and discussion of the results obtained from the measurement and simulation process;
- Chapter 5 – Conclusion and Future Research: This chapter presents the final considerations and suggestions for future work.

2 THEORETICAL FRAMEWORK

This section presents the theories, concepts, and models used in this work. It is a fundamental part of the thesis as it prepares the reader for a better understanding of what will be presented.

2.1 MICROWAVE SENSORS

Microwave sensors are highly specialized devices that operate in the range of 0.3 to 300 GHz and are capable of detecting and identifying samples based on their dielectric characteristics. Each sample presents specific electrical characteristics that determine how they behave in the presence of an electromagnetic field [31].

The electrical permittivity ε_f, magnetic permeability μ_f, and electrical conductivity σ_f are some of the intrinsic properties that define the behavior of electromagnetic waves of these samples, together with Maxwell's equations and boundary conditions. In general, these values are complex and vary with frequency; thus, it is essential to consider these characteristics when designing microwave sensors in order to optimize sensing systems [31].

2.2 COPLANAR LINE SENSORS

Coplanar lines, also known as coplanar waveguides (CPW), are structures with a specific design consisting of a conductor line of width *w* and thickness *t* printed on a substrate with relative permittivity ε_r and height h. In addition, on both sides of the conductor line, other return conductors are present, separated by a distance *G*. It is worth noting that the three conductors are in the same plane, which is a fundamental characteristic of these devices, coplanarity [32]. This configuration can be visualized in Figure 1, which graphically illustrates the structure of the coplanar waveguides.

Figure 1 – CPW Structure

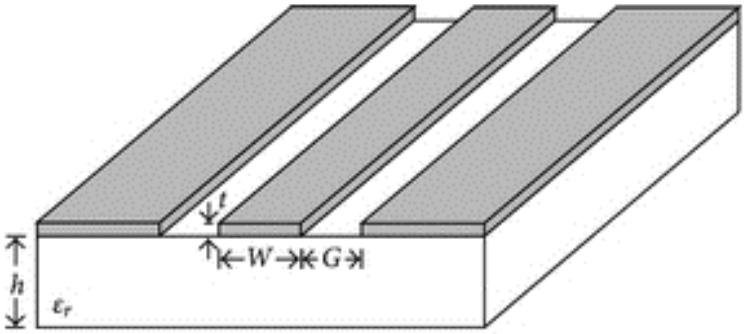

Source: Adapted From [33]

They present a configuration in which the conductors are located in the same plane, allowing the electric and magnetic fields to have less confinement than if they were in opposite planes, resulting in greater sensitivity to external elements [34]. This characteristic can be observed in Figure 2, which illustrates the distribution of electric and magnetic fields in the CPW structure. Such sensitivity is an important aspect in the application of CPW sensors since variations in the dielectric characteristics of the material to be analyzed can significantly affect the distribution of electromagnetic fields within the structure, resulting in a change in the sensor response.

Figure 2 – Transverse view of the distribution of electric and magnetic fields for a CPW line

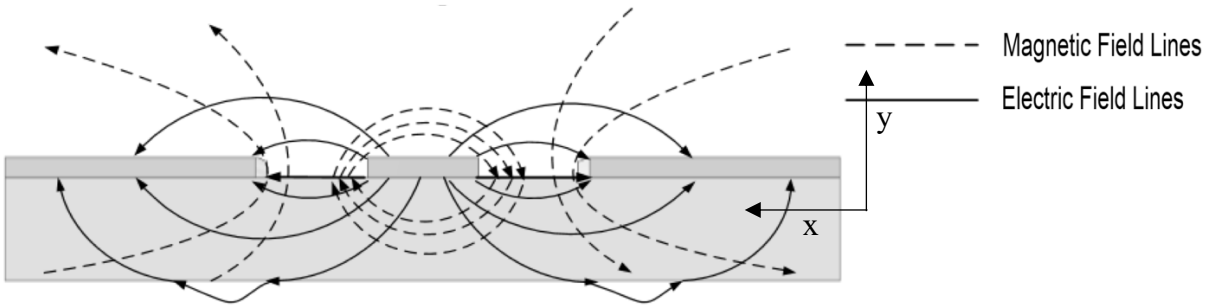

Source: Adapted From [35]

CPW structures have been widely used as sensing devices in various applications. For example, in [36], a CPW sensor with an interdigital capacitor resonator operating between 5 and 7 GHz was proposed for the characterization of chemical solvents. The sensor showed a shift in its resonance frequency of about 24 MHz for every 0.1 variation in the electric permittivity of the sample. In addition, the authors of [37] developed a planar CPW sensor for detecting adulteration in oil samples through perturbation in the S_{21} response of the system. In

[38], a CPW sensor coated with a metal oxide composite film was successfully employed for sensing ambient humidity.

2.2.1 Electromagnetic theory

Ideal coplanar waveguide structures have infinitely thick substrates and two infinitely wide grounding lines. However, in practice, a CPW is implemented with a substrate that has a finite thickness *h*, sometimes with metallization on the back; the grounding lines also have a finite width *W*, and although the conductors are very thin, they have thickness *t*. The width of the central conductor, the separation width between the central conductor and the coplanar lines *G*, and the thickness and relative dielectric permittivity ε_r of the dielectric substrate determine the characteristic impedance, effective dielectric permittivity, and attenuation of a CPW [39]. This can be seen in Figure 1.

At low frequencies, energy is transmitted along the CPW structure as an electromagnetic wave with a field configuration that closely resembles a transverse electromagnetic (TEM) mode; thus, it is assumed that the quasi-TEM mode propagates along the structure. As the frequency increases, the quasi-static estimate cannon be made, causing higher order modes to propagate along the CPW structure due to the nonzero longitudinal component of the magnetic field [40].

2.2.1.1 Propagation at microwave frequencies

The Maxwell's equations govern the propagation of electromagnetic waves along a coplanar waveguide. Figure 2 illustrates the distribution of the electric and magnetic fields in the cross-section of this type of waveguide. Considering a lossless dielectric substrate, the magnetic field satisfies the curl of Maxwell's equations, which can be expressed by Equation 1 [39]:

$$\nabla \times \vec{H} = \varepsilon_r \varepsilon_0 \frac{\partial \vec{E}}{\partial t} \tag{1}$$

Where $\vec{H}$ and $\vec{E}$ correspond, respectively, to the magnetic and electric fields at a given instant in time *t*.

Equation 2 is obtained from Equation 1 by considering the continuity of the tangential component of an electric field across the interface between air and the dielectric:

$$\varepsilon_r \frac{\partial H_{z,air}}{\partial y} - \frac{\partial H_{z,dielectric}}{\partial y} = (\varepsilon_r - 1)\frac{\partial H_y}{\partial z} \quad (2)$$

Where the subscript letter indicates the direction of the field component, and the names indicate the location of that component in the structure.

Equation 2 is shown to have a nonzero right-hand side, which implies the existence of a longitudinal component of the magnetic field. The magnetic field cannon is contained in the transverse plane. It is observed that CPW supports not only TEM modes but also hybrid modes that are superpositions of TE and TM modes. Additionally, when there is dielectric inequality along the CPW, propagation of higher order modes called "surface wave modes" occurs [41].

The dominant mode of the CPW, which refers to propagation along the line, approaches the TEM mode. The CPW has a low rate of electromagnetic energy leakage due to the existence of only transverse components of the electric and magnetic fields. However, in surface wave modes, the longitudinal components of the electric and magnetic fields are present and contribute to energy dissipation in the substrate [41].

The existence of the longitudinal component of the magnetic field results in the inclination of the magnetic vector toward propagation, and consequently, the Poynting vector points toward the substrate, as illustrated in Figure 3. Thus, electromagnetic energy is dissipated from the CPW to the substrate. At microwave frequencies, the CPW does not support the pure TEM mode, which requires a complete analysis of the waves [39].

Figure 3 – Transverse view of the distribution of propagation components of the electric and magnetic fields for a CPW line

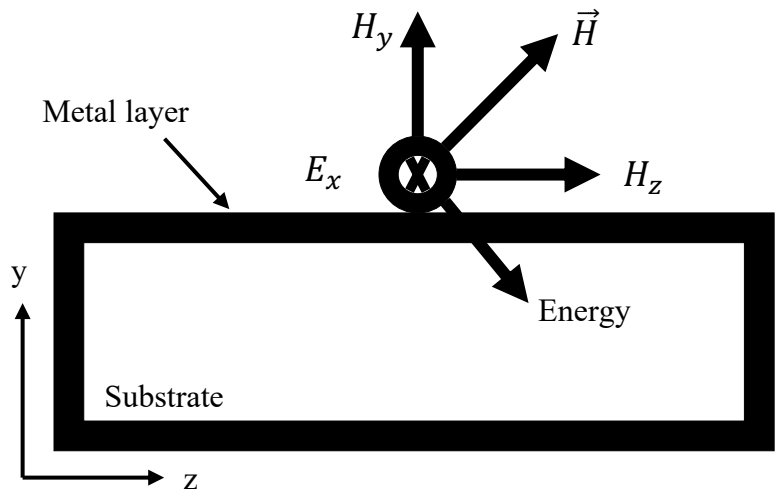

Source: Adapted From [35]

Several mathematical methods are available to perform this analysis; however, in this thesis, 3D electromagnetic simulation software using the finite element method was used. This software is capable of automatically calculating the necessary results during the simulation.

2.2.1.2 Attenuation of the propagated wave

The design of sensors requires careful observation of the attenuation parameter of the response. For CPW sensors, the electromagnetic wave that propagates through the structure experiences attenuation due to three main factors: conductor losses, dielectric losses, and radiation losses [42]. This design focuses on conductor losses, and therefore, this factor will be analyzed in more detail below.

The total attenuation of the wave along the CPW is significantly affected by conductor losses, which are caused by electrical resistance. This is because the value of the electrical conductivity of the metallization is finite. Imperfections in the manufacturing process, such as surface roughness, contamination, and impurities in the conductor material, are factors that contribute to electrical resistance. In addition, variation in the geometry of the conductor, such as the width and thickness of the trace, can also influence conductor losses [42].

For microwave frequencies, the conducting lines of the CPW have an electrical resistivity R_s inversely proportional to the electrical conductivity value σ and the skin depth δ_s of the metal. The total resistance of the CPW can be determined by Equation 3 [39]:

$$\mathrm{R} = R_s \frac{l}{G} \tag{3}$$

Where l is the length of the conductor line.

The value of conductor loss α_c, in cases where the CPW has a ground plane, is given by Equation 4 [43]:

$$\alpha_c = 4.88 \times 10^{-4} R_s \varepsilon_{eff} Z_0 \frac{P'}{\pi G}\left(1 + \frac{W}{G}\right)\left\{\frac{\frac{1.25}{\pi} ln\frac{4\pi W}{t} + 1 + \frac{1.25t}{\pi W}}{\left[2 + \frac{W}{G} - \frac{1.25t}{\pi G}\left(1 + ln\frac{4\pi W}{t}\right)\right]^2}\right\} \tag{4}$$

Where P' is a geometry-dependent parameter.

2.2.2 Physical dimensions and S parameters

The S parameters of a CPW, which refer to the reflection and transmission coefficients of the electromagnetic wave along the structure, are directly related to the physical dimensions of the structure, such as the width of the track, spacing between the track and ground lines, substrate thickness, and length of the line [44]. Therefore, it is essential to carefully consider the physical dimensions of the CPW during the design and fabrication of the structure to ensure the desired performance.

The reflection coefficient (S_{11}) is an important parameter for evaluating the amount of energy reflected back to the source when an electromagnetic wave is transmitted through a transmission line, such as CPW. This parameter is mainly affected by the characteristic impedance of the line and the width of the track. The characteristic impedance is a property of the transmission line that describes the resistance offered by the line to the passage of an electromagnetic wave. The width of the track also affects S_{11} since the characteristic impedance is directly proportional to the width of the track [45].

The expression for the characteristic impedance is shown in (5) [16],

$$Z_0 = \frac{30\pi}{\sqrt{\varepsilon_{eff}}} \frac{K(k\prime)}{K(k)} \tag{5}$$

K(k) is the complete elliptic integral of the first kind, ε_{eff} is the effective permittivity, and *k* is the ratio between the central conductor and the distance between conductors, as defined by equation (6) [46].

$$k = \frac{W}{W+2G} = \sqrt{1-k'^2} \tag{6}$$

For generic values of *w*, such as 1, 2, or 3, the values of *k* are known and can be found in tables, but they can also be calculated using equations (7) and (8) [47].

For $0 \leq k \leq \frac{1}{\sqrt{2}}$:

$$\frac{K(k)}{K(k\prime)} = \frac{1}{\pi} ln\left(2\frac{1+\sqrt{k}}{1-\sqrt{k}}\right) \tag{7}$$

For $\frac{1}{\sqrt{2}} \leq k \leq 1$:

$$\frac{K(k\prime)}{K(k)} = \frac{1}{\pi} ln\left(2\frac{1+\sqrt{k\prime}}{1-\sqrt{k\prime}}\right) \tag{8}$$

The transmission coefficient S_{21} represents the signal loss or attenuation that occurs along the transmission path between the input and output of a signal transmission device or

system. It is a commonly used scattering parameter in circuit and communication systems to characterize the transmission capability of a device or system [48].

This attenuation is affected by various factors, such as the width of the center line, the spacing between the center line and the coplanar lines, the length of the line, and the relative permittivity ε_r of the substrate [42].

The width of the centerline has a direct influence on insertion loss. Increasing the width of the line can reduce insertion loss because it decreases the conductor resistance, resulting in less wave attenuation. However, excessive widening of the trace can lead to excessive coupling between the centerline and coplanar lines, which can increase the insertion loss [42].

By reducing the distance between the centerline and the ground lines in a CPW, there is an increase in the capacitance of the centerline and a decrease in the inductance. This effect decreases the characteristic impedance of the CPW and consequently decreases the insertion loss. On the other hand, when the spacing is increased, there is a decrease in capacitance and an increase in inductance, resulting in an increase in the characteristic impedance and therefore higher insertion loss. An optimum distance should be designed [42].

The length of the line must also be observed, as the longer the length, the greater the attenuation and therefore the greater the insertion loss. When analyzing the value of the dielectric constant ε_r, we see that as ε_r increases, the capacitance of the CPW center line also increases, resulting in a decrease in the CPW characteristic impedance. This can increase insertion loss as part of the energy is lost due to coupling with the ground line [39].

On the other hand, when ε_r decreases, the capacitance of the CPW center line decreases, resulting in an increase in the CPW characteristic impedance. This can decrease insertion loss as less energy is lost due to coupling with the ground line [38]. All of these variables must be considered and modeled when designing a CPW sensor.

2.3 DMMP GAS

DMMP (Dimethyl methylphosphonate) is a colorless and odorless liquid with the chemical formula $C_3H_9O_3P$. This highly toxic and flammable organic compound is often used as a simulant for chemical warfare agents for testing protective equipment and sensors. DMMP has a boiling point of 188°C, a melting point of -76°C, and a density of 1.192 g/cm³ at 20°C. Furthermore, it is soluble in water and polar organic solvents but poorly soluble in nonpolar solvents [49]. Figure 4 shows the chemical structure of DMMP gas.

Figure 4 – Chemical structure of DMMP gas

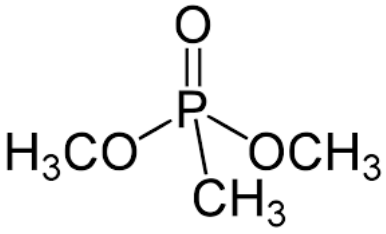

Source: Adapted From [49]

Other types of gases such as diisopropyl fluorophosphate (DFP), triethylphosphate (TEP) and diisopropyl methylphosphonate (DIMP) were initially employed for the simulation of toxic agents like Sarin, however, DMMP gas is currently the most widely used. One of the main reasons is that DMMP gas is less toxic, which allows for greater ease of use compared to the others [50].

DMMP and sarin exhibit chemical similarities, both having a phosphate group and a methyl group. During decomposition, both attach to the surface of metal oxides through their phosphorous oxygen, resulting in bidentate structure. However, sarin contains a fluorine atom instead of a methoxy group in DMMP. In reaction with the surface, the methoxy group is cleaved and protonated to generate methanol, forming methyl methylphosphonate (MMP) and then the second methoxy group is cleaved to form methylphosphonate (MP). This makes DMMP gas less toxic [51]. In Figure 5, it is possible to see the chemical structure of Sarin gas.

Figure 5 – Chemical structure of Sarin gas

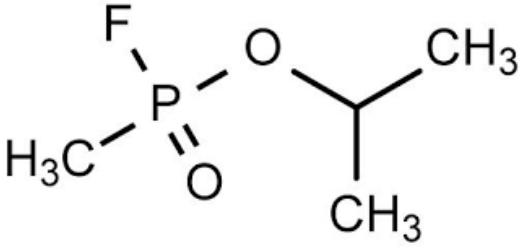

Source: Adapted From [51]

The similar reactions between DMMP and Sarin provide important insights into the reactivity of metal oxides with respect to Sarin. This is significant because these oxides play a crucial role in the decomposition of chemical warfare agents and simulants such as DMMP due to their catalytic ability. In order to develop detection systems and sensors for chemical warfare agents, studies are being conducted to understand the complex reactions that occur during the adsorption of DMMP vapors on the surface of metal oxides [51].

2.3.1 Palladium as a metal oxide

Palladium oxide (PdO) has been widely investigated as a material sensitive to DMMP gas. This material is attractive due to its catalytic and electrical properties, which can be leveraged to improve the sensitivity and selectivity of sensors [52].

Palladium oxides are chemical compounds that comprise palladium and oxygen atoms. Three palladium oxides are frequently encountered: PdO, Pd2O3 and PdO2. Generally, these compounds are obtained by the oxidation of palladium with oxygen or by heating other palladium compounds in the presence of air [53].

Palladium (Pd) is a metallic transition chemical element of group 10 in the periodic table with atomic number 46. It has silver white, malleable, ductile, corrosion resistant, and high electrical conductivity. It is a relatively scarce element in the Earth crust, found mainly in copper-nickel ores. Its applications include catalysis, jewelry industry, electronics, and dentistry [53]. Figure 6 shows the oxide in its pure form in laboratory setting.

Figure 6 – Palladium oxide

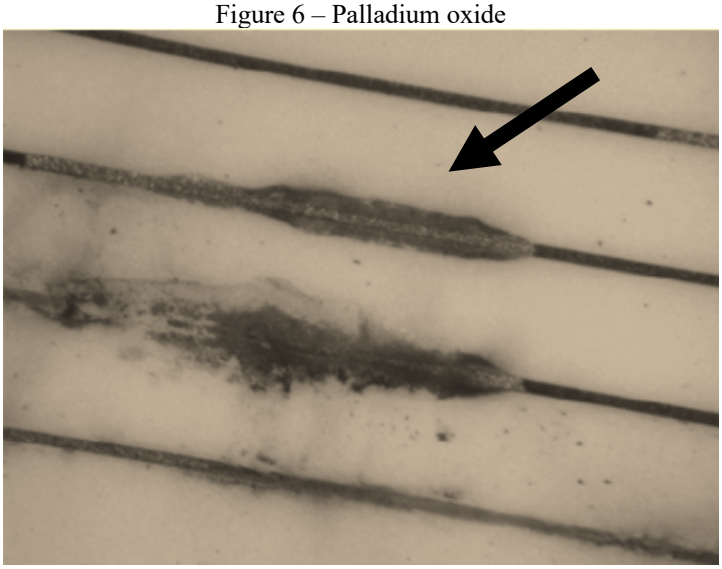

Source: Adapted From [54]

One of the scientific publications that has devoted in-depth research on the use of palladium as a material for DMMP gas detection is the reference scientific article [52]. This article describes a method for detecting DMMP vapor using a double-layer phthalocyanine-palladium structure. Phthalocyanine is an organic compound used as sensitive material in gas sensors due to its ability to adsorb gas molecules. Palladium, on the other hand, has been widely used as a catalyst in chemical reactions.

The double-layer phthalocyanine-palladium structure consists of a phthalocyanine layer deposited on a palladium layer. When exposed to DMMP vapors, the phthalocyanine adsorbs the DMMP molecules, which leads to the change of electrical resistance of the phthalocyanine-palladium double-layer. This change can be measured and used to detect DMMP vapors. In the graph of Figure 7, it is possible to see the relationship presented by the article between resistivity in $M\Omega$ and the concentration of DMMP in parts per billion (ppb) as the gas concentration increases and decreases.

Figure 7 – Double-layer phthalocyanine-palladium resistance vs DMMP concentration

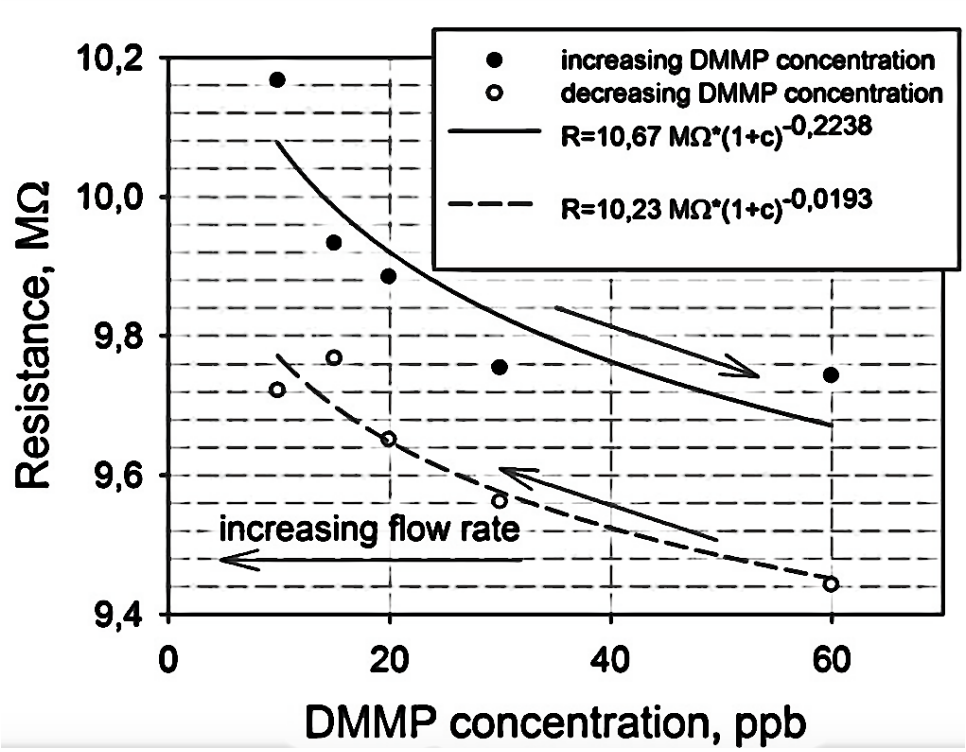

Source: Adapted From [52]

The study showed that the double layer structure of phthalocyanine-palladium exhibited high selectivity and sensitivity for detecting DMMP vapors even at low concentrations. for this structure, as the gas concentration was increased, the resistance value of the structure decreased, meaning that the vapor generated an increase in the conductivity of the palladium.

3 MATERIALS PROCEDURES

The experimental part of this work was carried out in two stages, namely:

- First stage: design of a CPW sensor, from material selection to simulation attempts;
- Second stage: fabrication, measurement of the prototype, and processing of the results.

3.1 PROJECT MATERIALS

In this project, DMMP gas was used as a gaseous agent to simulate toxic gases. As seen, the properties of this gas are similar to those of toxic gases. The careful selection of materials is a crucial step in the design of gas sensors. According to studies in [55], metal oxides have greater sensitivity for this purpose. The choice of ideal metal involves various factors such as the chemical interaction with target gas, chemical stability, ease of processing, sensor sensitivity and selectivity. The careful analysis of these factors allowed to select the most suitable material for sensor fabrication.

In [56], a sensor based on metal palladium was analyzed, showing good sensitivity to DMMP at concentrations between 10 and 60 ppb. This concentration level is quite low, which proves high sensitivity. This material also exhibited low resistance properties and stability at room temperature. Palladium has a standard electrical conductivity of 10^7 S/m. Figure 8 shows a picture of a palladium metal film.

Figure 8 – Thin film of palladium

Source: Adapted From [55]

Palladium was previously employed as a thin metal layer on various substrates. In Figure 9, a microscopic view illustrates the adhesion of a palladium particle on a TiO_2 substrate [57].

Figure 9 - Microscopy of a palladium molecule on a TiO2 substrate

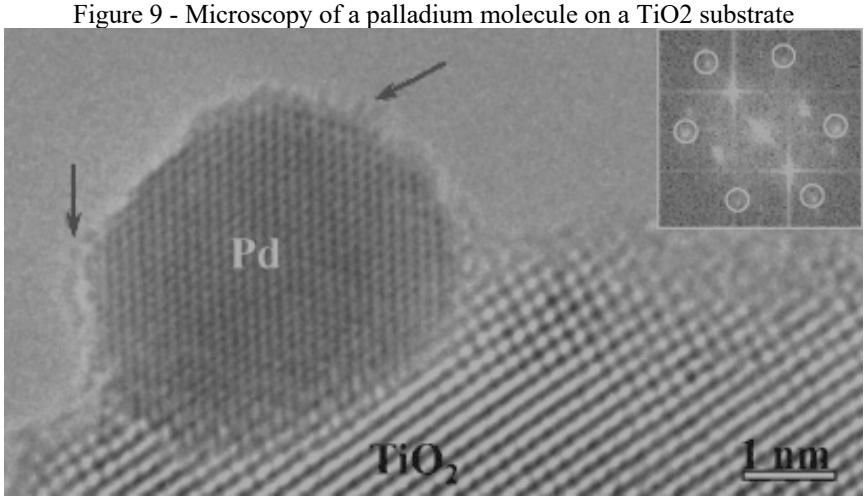

Source: Adapted From [57]

After palladium was chosen as the metal to be used in the CPW sensor, the next step was to determine the substrate to be used in the sensors.

The chosen material for substrate was fused quartz. Fused quartz has been used in the literature as a substrate for gas sensors. In [58], quartz was used as a substrate for a highly accurate NO_2 gas sensor. In [59], a hydrogen gas sensor based on zinc oxide was tested for two different substrates, quartz, and PET, and it was found that quartz yielded good results due to its physical properties (operates at room temperature, better adhesion to metal deposition, and rigidity). Additionally, quartz is a relatively low-cost material [60] and has low dielectric loss at microwave frequencies, which means that it can support microwave signal propagation with less energy loss [61].

In Figure 10, a flat and thin quartz wafer, similar to the one used in the project, can be seen.

Figure 10 – Quartz wafer

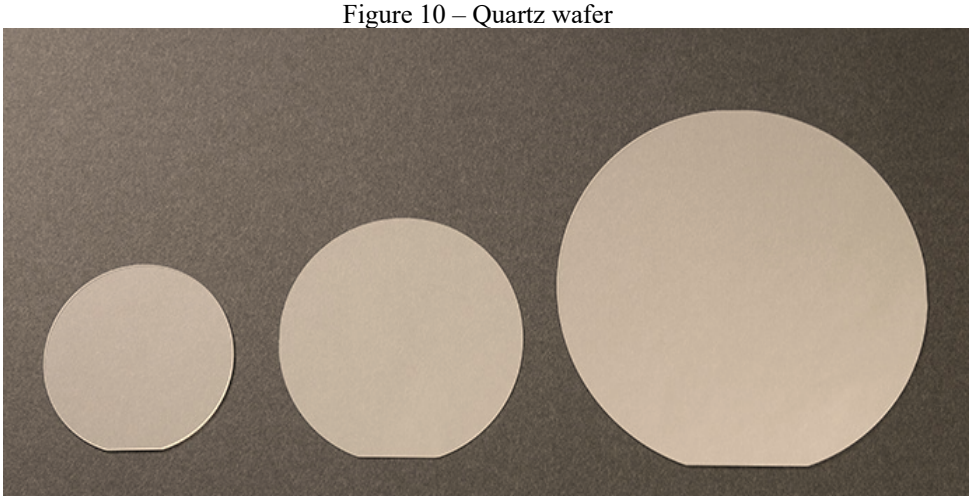

Source: Adapted From [60]

The study by [59] highlighted the smooth surface exhibited by the quartz substrate, which imparts the desired characteristics for this project. This analysis can be observed in Figure 11.

Figure 11 - Microscopic view of a quartz wafer at two different scales.

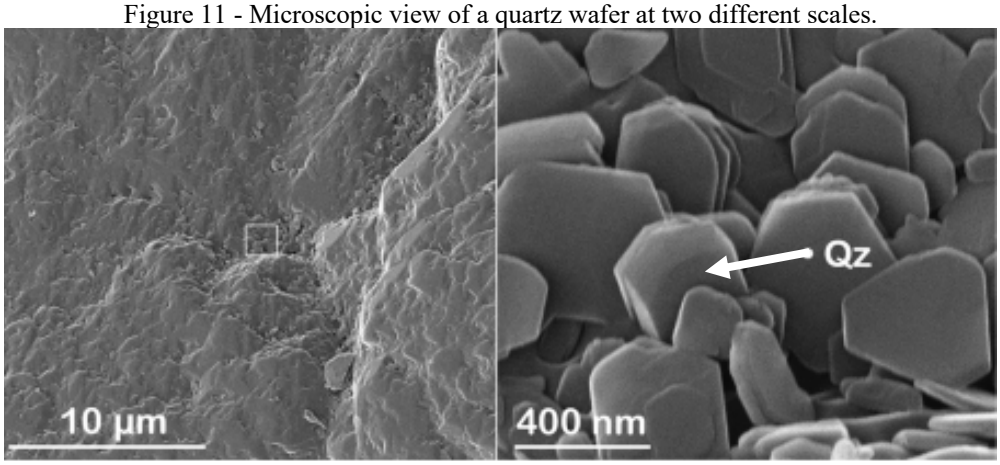

Source: Adapted From [61]

A consider for the sensor design was the available connector for measurement. The connector model used was Anritsu® 3680 V with frequency range from DC to 65 GHz. This connector is a popular universal test device because of its high precision and being a push-on coaxial connector. Push-on connectors facilitate quick connection and disconnection in high-frequency measurements [62]. Knowing the connector before designing the filter is important to determine the size limits and minimum and maximum supported thicknesses. The connector in a measurement environment can be seen in Figure 12.

Figure 12 – Anritsu® 3680V universal test device in operation

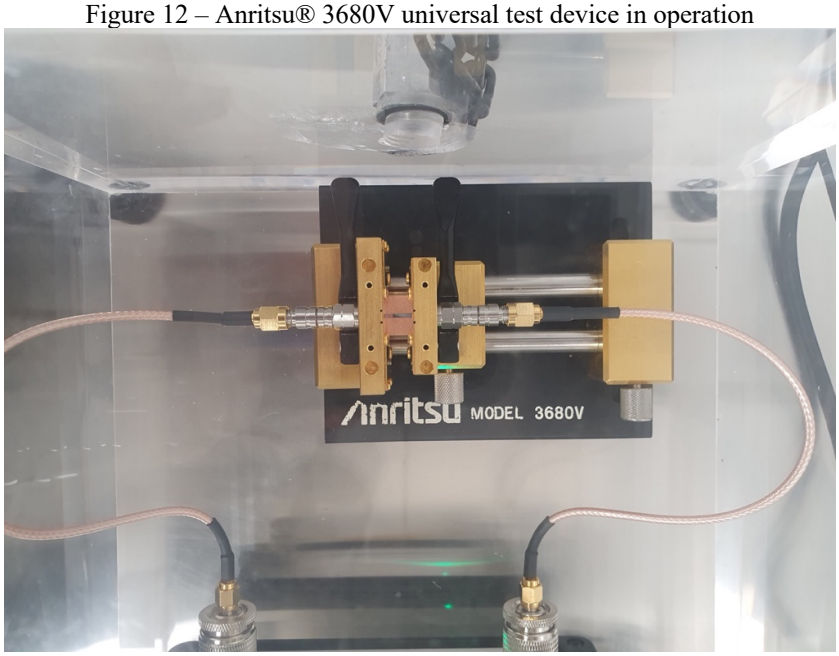

Source: The Author (2023)

3.2 OPERATING PRINCIPLES OF THE SENSOR

The operating principle of a gas sensor is based on the variations in the conductivity of palladium when exposed to DMMP gas. The idea is inspired by a previous work [59] and the behavior of the sensor is evaluated through variations in the S parameters. Detection is based on the interaction of the gas with the surface of palladium, which leads to a change in electron mobility in the metal and consequently a change in the electrical conductivity of palladium. This process of gas adsorption on the surface of palladium is highly selective and sensitive to the presence of DMMP gas. The variation in electrical conductivity is then detected by the sensor and used to identify the presence of gas, thus allowing for a rapid response in emergencies [63]. A schematic can be seen in Figure 13.

Figure 13 – Sensor operation setup

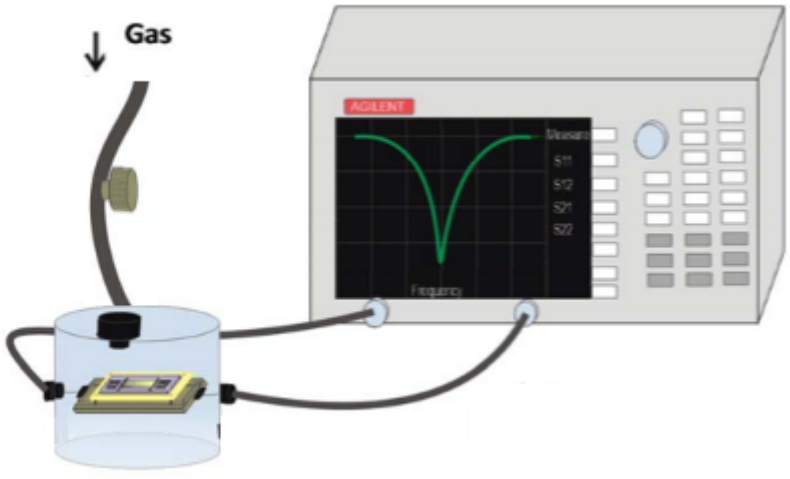

Source: Adapted From [58]

3.3 COMPUTATIONAL MODELING

The EM simulation tool used was the software CST® Studio. CST® Studio is one of the most sophisticated and popular electromagnetic analysis tools available today. It is widely used to simulate microwave devices and antennas, such as planar microwave sensors. The simulation using CST® Studio allows the investigation of sensor performance in various situations and optimization to meet detection demands. Additionally, simulation offers a thorough understanding of the sensor behavior and underlying physics, allowing precise adjustments to the design to achieve ideal sensitivity and selectivity [64].

In the modeling of the sensor, specific materials and dimensions were used. The sensor was developed in the simulation environment using a CPW structure. The choice of materials employed in the sensor construction achieved the necessary electromagnetic properties for detecting the signal of interest. The dimensions employed in the sensor construction were determined according to the project specifications to ensure proper device performance.

The used materials and their dimensions were as following:

- Conductive metal: 40 ηm of Palladium.
- Substrate: 525 μm of fused Quartz;
- Ground plane: 35 μm of Copper;
- Dimensions: 25 mm length by 7.2 mm width.

In Figure 14, it is possible to see the sensor designed in the simulation environment.

Figure 14 – Simulated CPW sensor a) Front view b) Side view

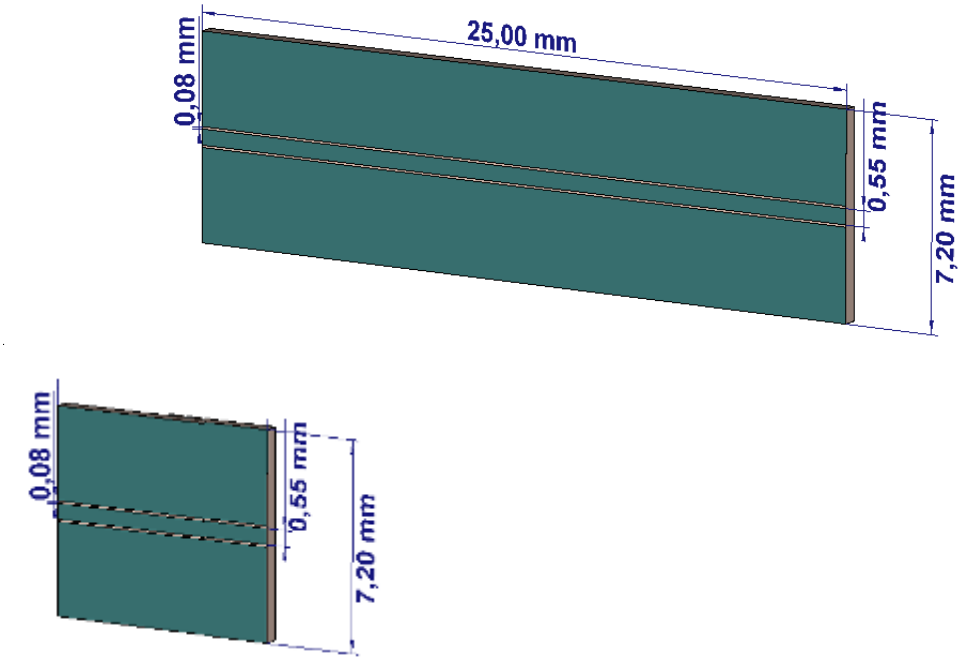

(a)

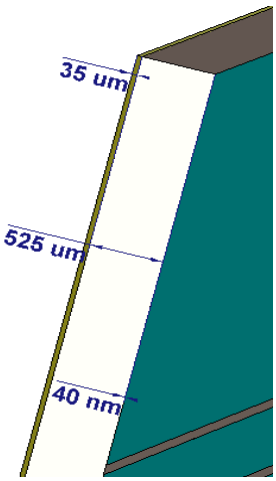

(b)

Source: The Author (2023).

Note that the thicknesses of the metal and substrate were established considering the limitations of the manufacturing processes, while the dimensions were optimized to ensure a satisfactory response of the sensor, maximizing the use of the available space on the quartz wafer.

An important aspect that deserves to be mentioned is the role played by the conductivity of palladium in the CPW sensor simulation. In this context, the conductivity of palladium was

considered as a variable parameter to be adjusted to reflect the expected variation of the electrical conductivity of palladium resulting from the interaction with DMMP gas. In this sense, the variation of palladium conductivity was incorporated into the simulation as a determinant factor to accurately model the behavior of the sensor in the presence of DMMP gas.

The main goal of the simulation is to obtain the S_{21} response of the S parameters over a wide operating range ranging from 0 to 15 GHz for the sensor containing palladium with standard electrical conductivity (i.e., under ideal conditions, without the presence of gases). Additionally, it is intended to investigate the S_{21} response in situations where there is variation in the electrical conductivity of palladium, allowing for simulation of an interaction between the gas and the sensor.

3.4 FABRICATION

The fabrication of the CPW sensor represents the most critical and specialized phase of this work. This procedure was carried out at the renowned Institut de Ciències Fotòniques (ICFO), whose expertise in the field of photonics is widely recognized (well know). The process consisted of depositing a palladium film onto a quartz substrate using a spin coating and lift-off technique.

This highly complex method requires millimetric precision and was used to ensure the quality and consistency of palladium film deposition on the substrate with the aim of producing highly sensitive and reliable CPW sensor. The successful execution of this process is essential to ensure the effectiveness of the sensor and the obtaining of precise and reliable results in the subsequent stages of this study.

The spin coating process is an extensively employed procedure for depositing thin films of material onto uniform and flat surfaces. This technique is based on the rotation of the substrate coated with the solution or suspension of the material to be deposited. During rotation, the centrifugal force causes a uniform distribution of the material on the substrate surface [65].

The main stages for developing a planar sensor using the spin coating method are as follows [65]:

- Substrate preparation: The quartz substrate is cleaned and treated to ensure that the surface is free of contaminants and ready to receive the deposited material;

- Solution preparation: The material to be deposited (palladium) was dissolved in a suitable solvent to form a solution. The concentration of solution and the rotation speed of substrate in the spin coating process will affect the thickness of the deposited layer;
- The deposition of the layer: The solution was placed on the substrate and spun at high speed to spread the solution over the surface of the substrate. The centrifugal force created during the process causes the solution spread uniformly and a thin and uniform layer is formed;
- Drying of the deposited layer: The layer is subjected to a suitable drying period;
- Sensor standardization: Spin coating is done with photoresist to make a mold by exposing the photoresist using a mask and mask aligner to define the mold pattern, then the sample is placed for e-beam metal evaporation of Pd over that mold and the substrate. Then the process of lift off is removing the photoresist mold using chemicals, which means, the mold detaches from the substrate and the Pd pattern is what we get;
- Final cleaning: the substrate is subjected to final cleaning to remove any residues from the solution or the lift-off process. A thin copper film was placed under the sensor to function as a ground plane.

Figure 15 shows the process flow of sensor manufacturing using the method described above.

Figure 15 - Process Flow of Spin Coating and Lift-Off

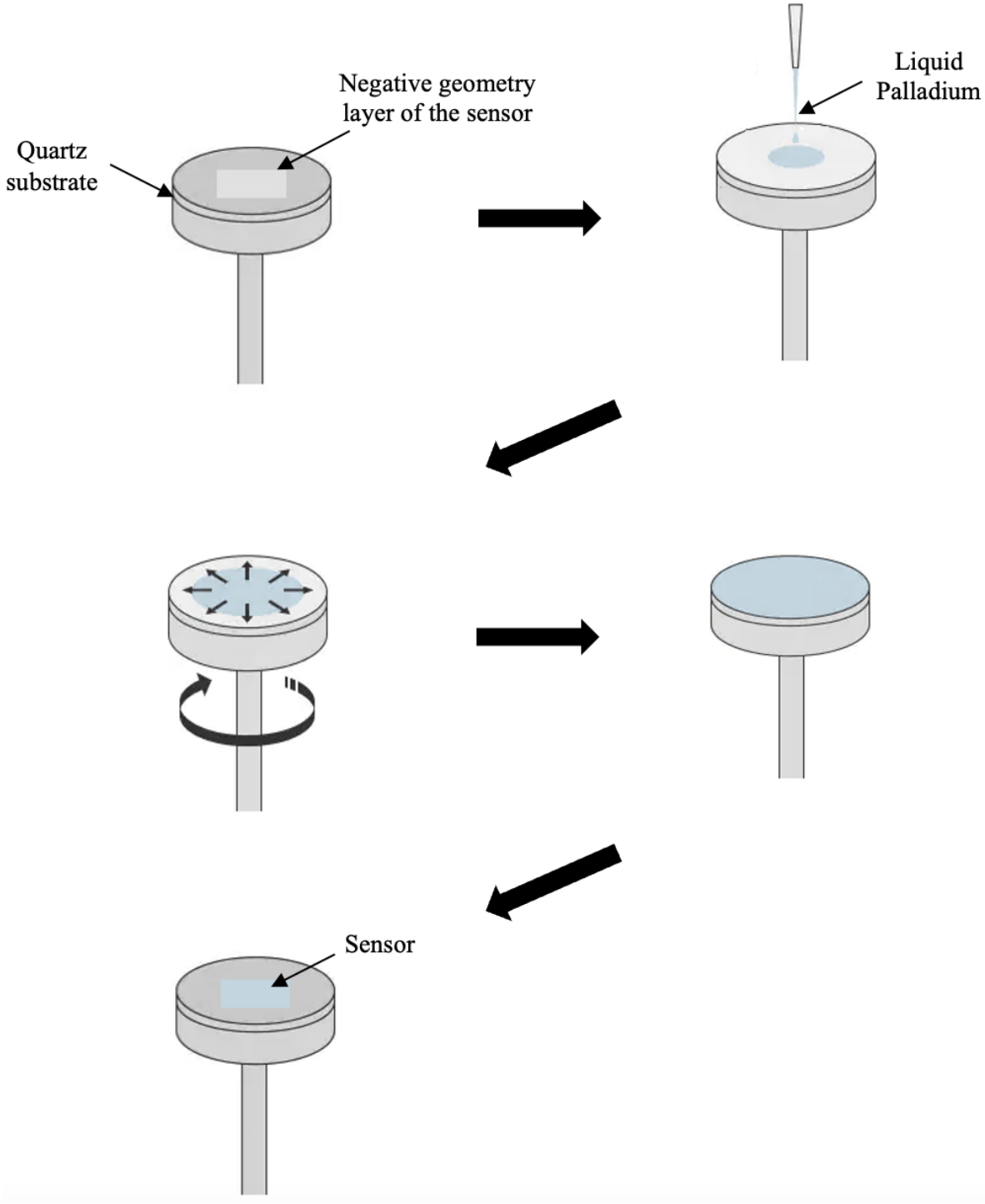

Source: The Author (2023).

After completing the procedures previously described, the sensor is ready for measurements complying with the previously defined specifications. Figure 16 shows the final structure of the sensor.

Figure 16 – Manufactured CPW sensor

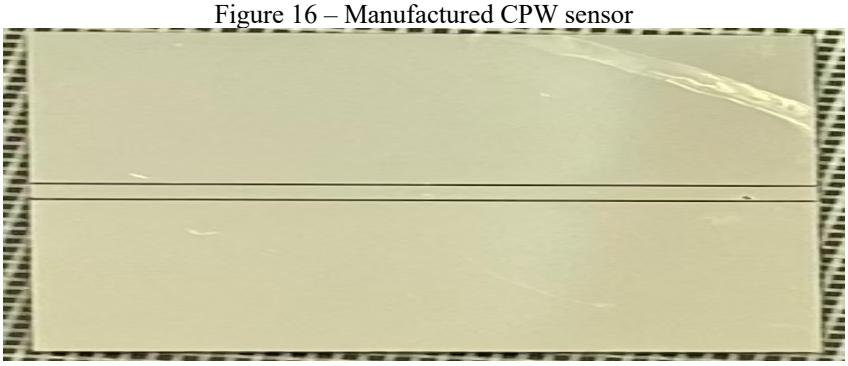

Source: The Author (2023).

3.5 MEASUREMENT AND DATA PROCESSING

The measurements required to evaluate the effectiveness of the sensor in detecting DMMP gas required the implementation of a highly controlled environment. In fact, it was necessary to conduct the measurements in facilities with a high level of security, precisely in the premises of the National Institute of Aerospace Technology (INTA), an institution linked to the Ministry of Defense of the Government of Spain.

The experimental arrangement used for the measurements consisted of the CPW sensor connected to the Agilent® E8361A vector network analyzer (measuring from 0 to 15 GHz) through an Anritsu® 3680V universal test device. In addition, the setup was equipped with a small tube designed to provide DMMP gas coming from a gas generator directly to the sensor. The strategic position of this tube near the top of the sensor allowed precise analysis of the interaction between gas and sensor. Figure 17 shows the setup in the measurement environment.

Figure 17 – Measurement setup

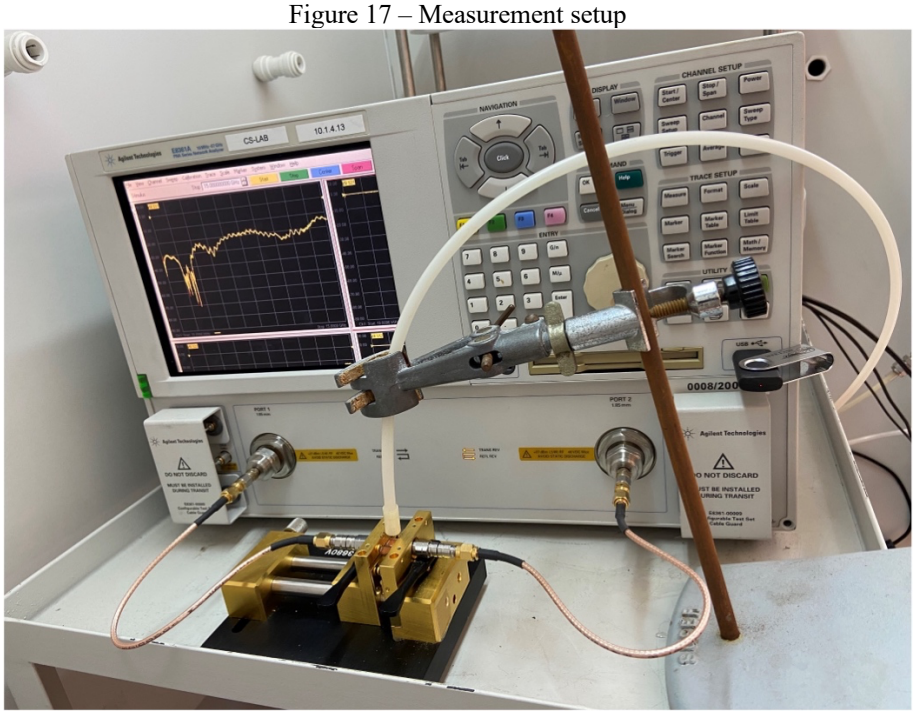

Source: The Author (2023).

The gas concentration of DMMP provided was kept at the lowest possible value, corresponding to 400 parts per million (ppm). the main objective of the project is to ensure the most accurate and sensitive detection of the gas in question.

During the measurements, the exposure time of the sensor to DMMP gas was carefully controlled and the experiment was repeated with several copies of the CPW sensor to ensure reproducibility of the results. In addition, the response of the S-parameters was monitored after the interruption of the DMMP supply to evaluate the sensors' ability to return to initial values.

The data acquired during the measurements were recorded directly by the network analyzer and stored for further analysis. However, raw data are susceptible to inherent measurement system noise, which can affect the accuracy of the results. To minimize these effects, it was necessary to perform preliminary data processing using smoothing techniques. For this purpose, a smoothing process was applied to the data obtained directly from the analyzer to improve the quality and reliability of the collected information.

Data smoothing techniques, also known as data filtering, involve applying an algorithm that reduces noise and fluctuations present in raw data obtained by a spectral network analyzer at microwave frequencies. These noises can be caused by various sources such as electromagnetic interference, electrical oscillations, and temperature fluctuations [66].

Data smoothing was performed by applying a Butterworth low-pass digital filter. This type of filter is designed to attenuate frequencies above a specified cutoff frequency while maintaining frequencies below that cutoff frequency. The choice of a Butterworth low-pass digital filter for this application is common due to its flat magnitude response properties, which means that the frequency response of the filter is constant over a certain frequency range. It is desirable to avoid unwanted signal distortions [67].

4 SIMULATION AND MEASUREMENT RESULTS

In the following section, the results obtained from both simulation and measurement processes are presented and discussed. These results were analyzed according to the operating conditions and characteristics of the sensor used to evaluate its efficiency in detecting DMMP gas:

4.1 SIMULATION AND ANALYSIS OF THE PREVIOUS CPW SENSOR

Initially, the considerations adopted in this project regarding palladium involved the use of a thickness greater than its skin depth value in order to minimize possible errors associated with the attenuation of the electromagnetic field in the material surface layer. This occurs because when using a thickness much smaller than the skin depth value, the amount of material responsible for attenuating the field in the surface layer can become too small, leading to incorrect simulation results [68].

To calculate the skin depth value of palladium for a frequency of 6 GHz, we used equation (9) [68]:

$$\delta = \sqrt{\frac{\rho}{\pi f_0 \mu_r \mu_0}} \tag{9}$$

Where δ is the skin depth value, ρ is the electrical resistivity of palladium at a value of 10.54 $\mu\Omega\ cm$, f_0 is the frequency in Hz, μ_r is the relative permeability at a value of 1, and μ_0 is the permeability of free space corresponding to $4\pi \times 10^{-7}$. Therefore, the skin depth value found was 2.109 µm.

An initial palladium thickness of 0.003 mm and a standard conductivity value of $9.71 \times 10^6\ S/m$ was used in the simulations. Figure 18 shows the simulated results of the S_{11} and S_{21} parameters for the initially proposed CPW sensor.

Figure 18 – Simulated S_{11} and S_{21} parameters for the CPW sensor with 0.003 mm of palladium

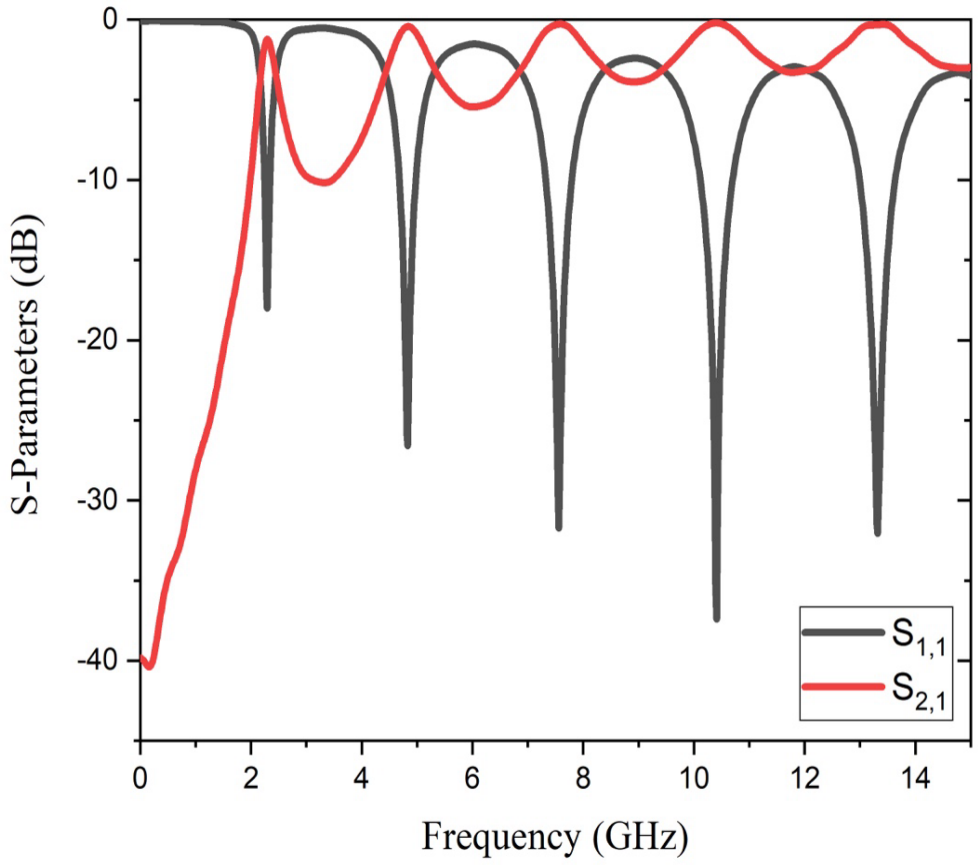

Source: The Author (2023).

The S_{11} parameter measures the reflection of an electromagnetic wave at the input port of a CPW sensor [69]. The parameter graph shows a step-like behavior, where peaks represent the signal reflected back to the input port of the sensor. These peaks are caused by resonances that occur due to the interaction between the signal and the sensor and with the medium in which it is immersed. The peaks are more attenuated with increasing frequency because losses tend to be higher [70].

The S_{21} parameter measures the transmission of electromagnetic waves through the CPW sensor. In the case of an ideal CPW sensor, the S_{21} parameter graph would be a horizontal line with a constant value of 0 dB, indicating that the transmitted power is equal to the received power [71].

In the case of a CPW sensor with losses, the S_{21} parameter graph shows a gradual decrease in amplitude with increasing frequency. This is due to losses in the sensor material

and transmission structure, which absorb part of the energy of electromagnetic wave and dissipate it in the form of heat.

In sensing applications, the interest is in detecting changes or disturbances in electromagnetic properties of the measured medium. For this reason, the analysis of the sensor response should focus on how it transmits or attenuates a signal when passing through the sample. In this context, the S_{21} response of the sensor is the most useful for analysis and it is the focus of this work.

The second analysis studied the behavior of S_{21} response for a variation of the palladium conductivity. This variation was carried out with the intention of simulating the conductivity changes that occur in the presence of damp gas. Two conductivity values were established apart from the initial value as an initial attempt. The double conductivity value, i.e., $1.942 \times 10^7\ S/m$, simulated the idea of damp gas increasing the conductivity of palladium, while half the conductivity value, i.e., $4.855 \times 10^6\ S/m$, simulated the case of gas decreasing the conductivity. This can be seen in Figure 19.

Figure 19 – S_{21} parameter of the CPW sensor for three values of electrical conductivity of palladium

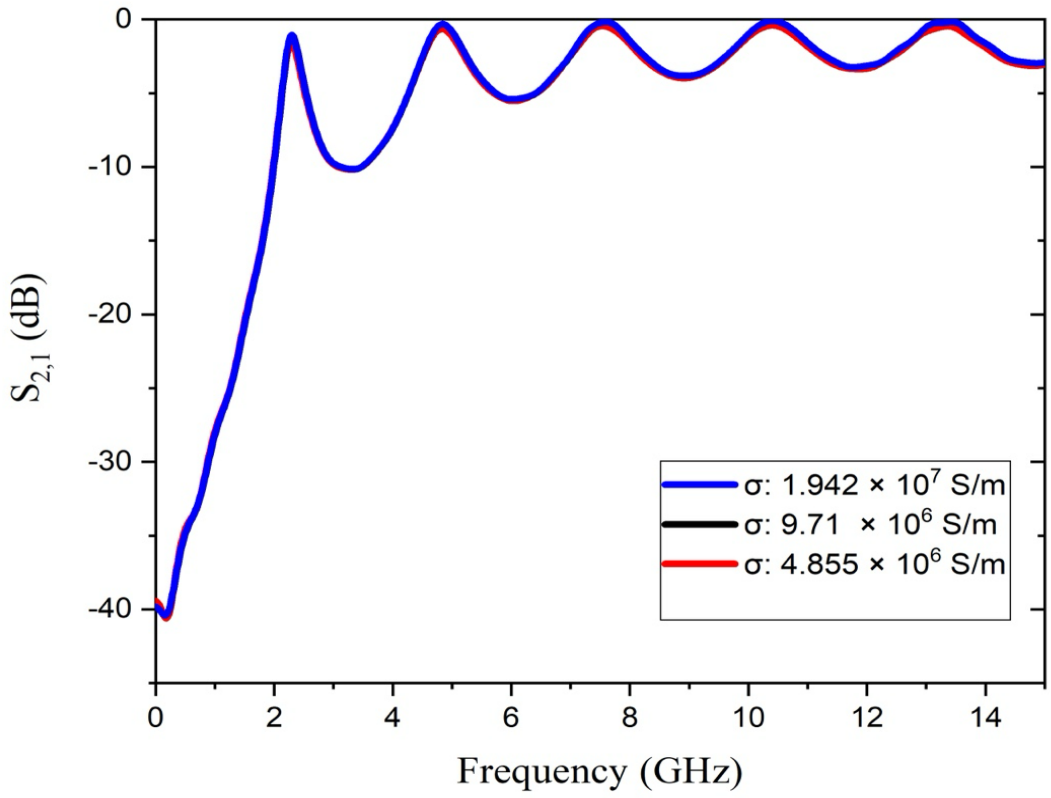

Source: The Author (2023).

Apparently, no significant changes were observed in the S_{21} response of the CPW sensor, but this is due to the frequency range chosen. However, as shown in Figure 20 by restricting the analysis to a more specific frequency range from 6 to 10 GHz, it was possible to observe a variation in the S_{21} response for a variation of palladium electrical conductivity.

Figure 20 – S_{21} parameter of the CPW sensor for three electrical conductivity values of palladium in a smaller frequency range

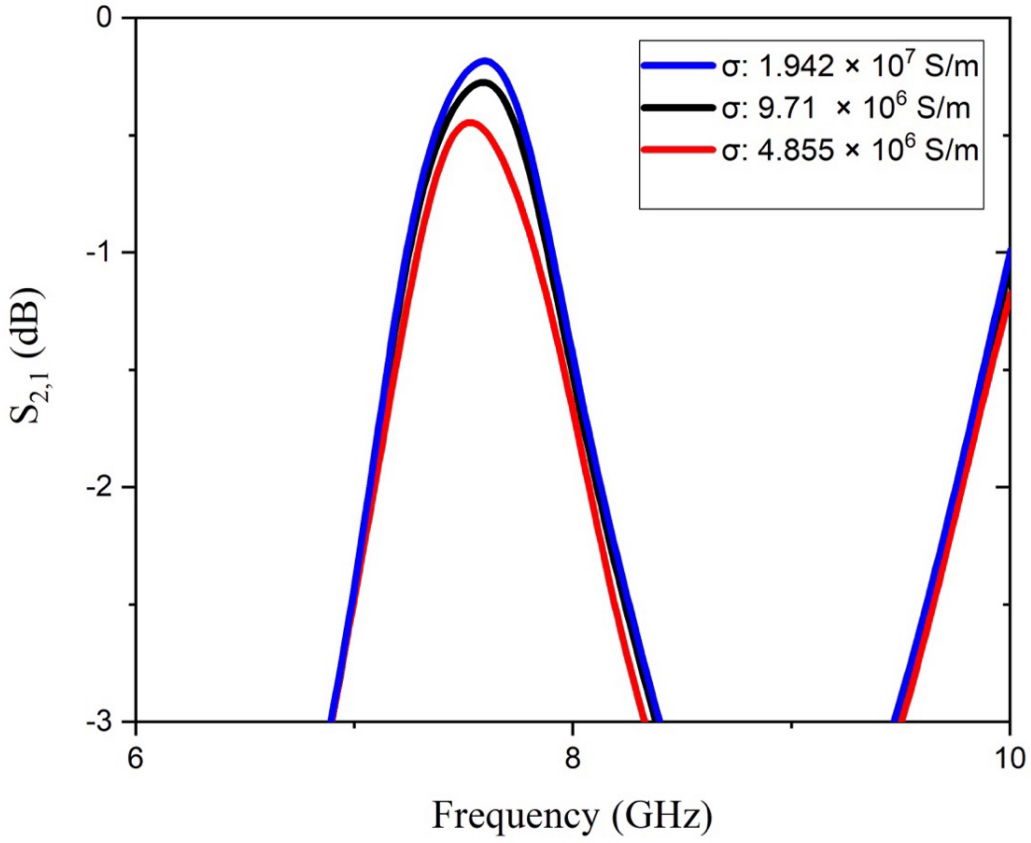

Source: The Author (2023).

Although it is a discrete change, a variation in the conductivity of palladium is noticeable in the S_{21} response of the CPW sensor. A difference of 0.10 dB was observed between the standard value and twice the conductivity and 0.2 dB between the standard value and half the conductivity. When the metal conductivity decreases, there is an increase in the attenuation of S_{21} response, indicating greater energy loss in the signal transmission through the sensor. On the other hand, when the metal conductivity increases, the attenuation of the S_{21} response decreases, indicating lower energy loss. This validates the initial idea of analyzing the electrical conductivity of palladium when used with a CPW sensor.

4.2 SIMULATIONS AND ANALYSIS OF THE 40 NM-PALLADIUM-CPW SENSOR

The limitations of the manufacturing process restricted the thickness of the palladium to 40 nm, which is significantly smaller than the skin depth of the material for the electric field. However, the reduced thickness does not affect the performance of the sensor. To evaluate the structure of the final sensor, simulations were attempted considering the actual thickness of 40 nm palladium.

During the simulation, it was observed that the software was unable to produce satisfactory results either showing no response or presenting incorrect responses as illustrated in Figure 21. As a possible cause of these anomalies, the metal thickness used in the sensor was identified, which apparently contributed to these unsatisfactory results.

Figure 21 – Incorrect simulated response for the CPW sensor with 40 nm of palladium

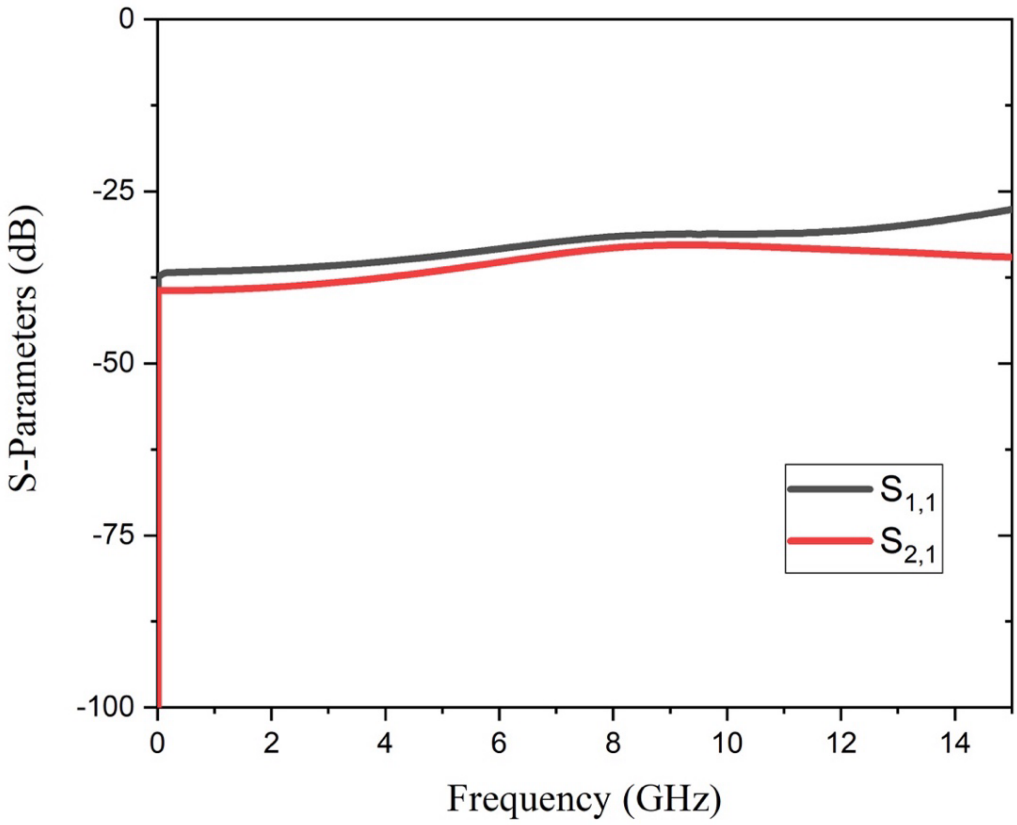

Source: From The Author (2023).

Now that the measurements of the 40 nm palladium device have been successfully carried out, as will be seen in the future, theories arise about the impossibility of simulating the sensor. This issue will be discussed in more detail later.

4.2.1 Skin depth effect

The skin depth, also known as penetration depth, is a fundamental property that influences the propagation of electromagnetic waves in conductive media [68]. In the case of a CPW sensor, the transmission of electromagnetic energy occurs through the electromagnetic field in the space between the sensor's transmission lines [72]. When the metal used in the sensor fabrication has a thickness significantly smaller than the skin depth, which is the depth at which the electromagnetic field is attenuated by 63%, the interaction between the electromagnetic field and the metal becomes quite distinct from what would occur if the thickness were greater.

Under these circumstances, the electromagnetic field is not completely absorbed by the metal and part of the field passes through the metal, propagating in the air or substrate and altering the energy transmission characteristics of the sensor. Since the mesh cannon be refined correctly, this can make the simulation more complex or even impossible, as energy transmission will not follow theoretical predictions and may generate unpredictable results.

4.2.2 Non-local response

The nonlocal response in the finite element method (FEM) occurs when the solution at a point of interest is influenced not only by local variables such as geometry, material properties, and boundary conditions, but also by variables at nearby points. This phenomenon is observed when the scale of the problem is comparable to the size of the finite elements used in discretizing the domain. When the finite elements are large compared to the spatial characteristics of the solution, the response can be affected by events occurring outside the element. To deal with this problem, the nonlocal response can be incorporated into the mathematical model through an additional correction that considers the interaction between nearby elements [73].

In the specific case of the CPW sensor with palladium, the metal thickness is very thin, which can result in a nonlocal response. This phenomenon can lead to errors in the simulation

of the sensor in CST Studio software, as it can be challenging to properly handle the additional correction required to account for the nonlocal response. Due to the significant increase in the number of degrees of freedom in the simulation, the software requires considerable processing power for analysis, which can be a limitation in the simulation. In addition, the implementation of this technique can generate inaccuracies in the results and increase the processing time of the simulation, factors that can impair the accuracy and efficiency of the simulation process.

Theories of non-local responses to nonlinearity problems have been previously described in the literature. The work presented in [74] introduces a variable known as the geometrical non-linear factor Λ(T), which is temperature, transmission linewidth and strip thickness dependent. This variable can be incorporated into the mathematical simulation model to address the issue of non-locality.

In this model, nonlinearity is embedded within the distributed inductance and resistance of the transmission line, as described below (10).

$$L(T,i) = L_0(T) + \Delta L(T,i), \quad R(T,i) = R_0(T) + \Delta R(T,i) \tag{10}$$

C (Capacitance) and G (Conductance) represent the ability to store charge and the ability to conduct electricity along the transmission line per unit length. The total current in the transmission line is denoted by i. T stands for temperature, while R_0 (Resistance) and L_0 (Inductance) are current-independent terms. These terms can be calculated using well-known formulas for microstrip transmission line parameters. According to (11), the nonlinear parts of inductance and resistance depend on the factor Λ(T), as described in [74].

$$\Lambda(T) = \frac{\int j^4 dS}{(\int j dS)^4} \tag{11}$$

Integration in (11) takes place along the cross-sectional area of the transmission line. Concerning the current distribution in thin-film transmission lines, a closed-form equation for Λ(T) in these transmission lines can be derived. After calculations and simplifications, we obtain an analytical expression for Λ(T) for any transmission line, considering temperature, transmission line width, and strip thickness, as indicated in (12).

$$\Lambda(T) = \frac{\left[\left(\frac{W^2 t}{8\lambda^2}\right)+\left(\left(\left(\frac{W^3}{2}\right)-\left(\frac{\lambda^2 W^2}{t}\right)\right)/\left(W^2-4\left(\left(\frac{W}{2}\right)-\left(\frac{\lambda^2}{t}\right)\right)^2\right)\right)+\left(\frac{W}{2}\right)arctgh\left(1-\left(\frac{2\lambda^2}{Wt}\right)\right)\right]}{t^3\left[Warcsin\left(1-\left(\frac{2\lambda^2}{Wt}\right)\right)+\lambda\sqrt{\frac{W}{t}}\right]^4} \quad (12)$$

Where W is the transmission line width, t is the thickness of the transmission line and λ is the london penetration depth.

4.3 MEASUREMENT AND DATA PROCESSING

Although it was not possible to perform a direct comparison with simulation results, experimental measurements were performed on the CPW sensor with 40 nm palladium, as it was initially observed that the variation in palladium conductivity could affect the S_{21} response of the sensor.

During the experiment, the CPW sensor was positioned below the DMMP gas source. Measurements of the sensor's S_{21} response were taken without the presence of gas, followed by measurements at time intervals of sensor contact with the gas, with values recorded at 0, 15, and 30 min of DMMP exposure. the concentration of DMMP used was 400 ppm and identical sensors were used in the measurements to increase the accuracy of the results.

The results extracted directly from the analyzer at the moments described above presented behavior that can be seen in Figure 22.

Figure 22 – Initial response extracted from the analyzer for the sensor with 40 nm of palladium and without contact with DMMP gas

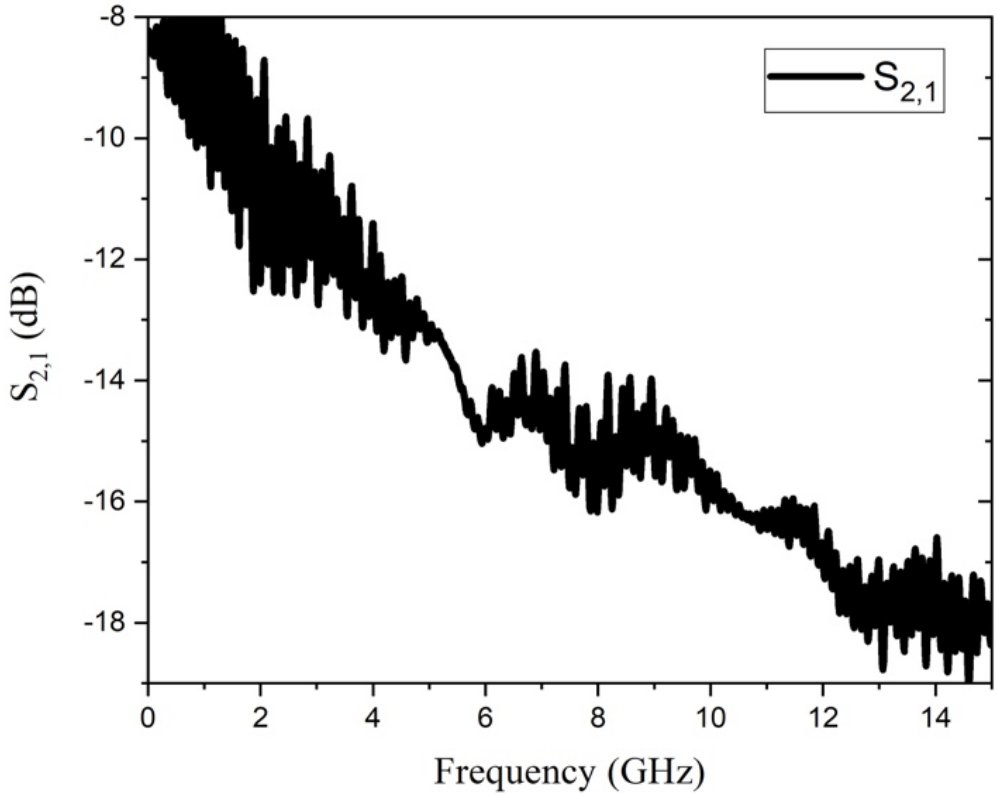

Source: The Author (2023).

As observed in Figure 22, the sensor response in the frequency range up to 15 GHz presented noise levels, which can compromise measurement accuracy. To overcome this situation, a data smoothing technique (smoothing method) was applied to obtain a response closer to the sensor's real behavior.

A sensor response can contain noise and fluctuations due to various factors, such as vibrations, electromagnetic interference, and temperature variations, affecting the accuracy and reliability of measurements. The smoothing technique, or digital filtering, is employed to reduce these noises and make the sensor response closer to the real one [67]. A Butterworth low-pass filter was used to attenuate high-frequency components responsible for noise and fluctuations and preserve low-frequency components corresponding to the sensor's real response.

Figure 23 illustrates the comparison between the measured S_{21} responses of the CPW sensor. It is possible to notice that the filtered S_{21} response is represented by the red line, while the noisy S_{21} response is shown by the black line.

Figure 23 – Comparison of filtered response vs response with noise for a) Frequency range between 0 and 15 GHz b) Frequency range between 6 and 10 GHz

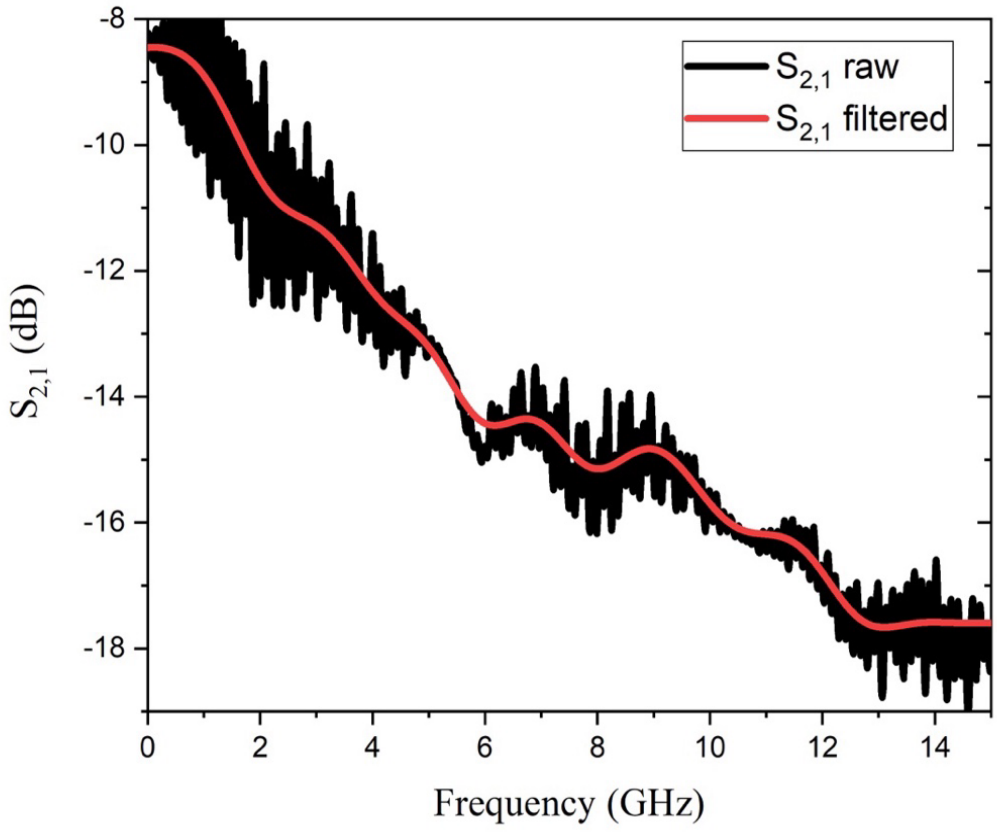

(a)

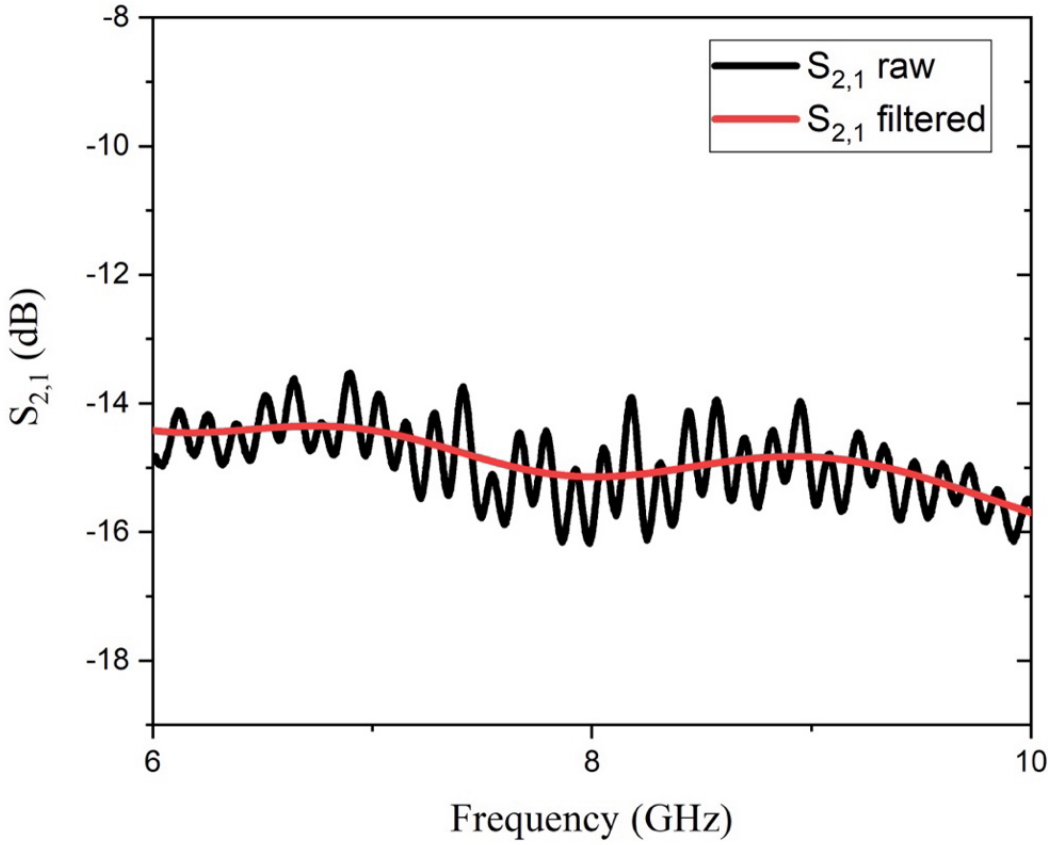

(b)

Source: The Author (2023).

The digital filtering procedure employed demonstrated efficiency in obtaining more linear responses for the S_{21} sensor both in its initial condition without presence of gas and after exposure to DMMP gas at intervals of 0, 15, and 30 min. The application of the filtering technique allowed the attenuation of the noise and fluctuations in the original measurements, making the responses more accurate and reliable.

After the procedures mentioned above were carried out, S_{21} response values were obtained for the sensor exposed to DMMP gas at intervals of 0, 15, and 30 min. These values allowed necessary comparisons for the analysis of gas-sensor interaction and the evaluation of the effectiveness of the sensor as a detection device.

In Figure 24, two graphs show the S_{21} responses for different frequency ranges. The first graph presents the response for frequencies between 0 and 15 GHz, while the second graph presents the response for frequencies between 0 and 10 GHz. This graphical representation allows a clear visualization of variations in sensor responses at different time intervals.

Figure 24 – Comparison of filtered response at four times: a) between 0 and 15 GHz b) between 6 and 10 GHz

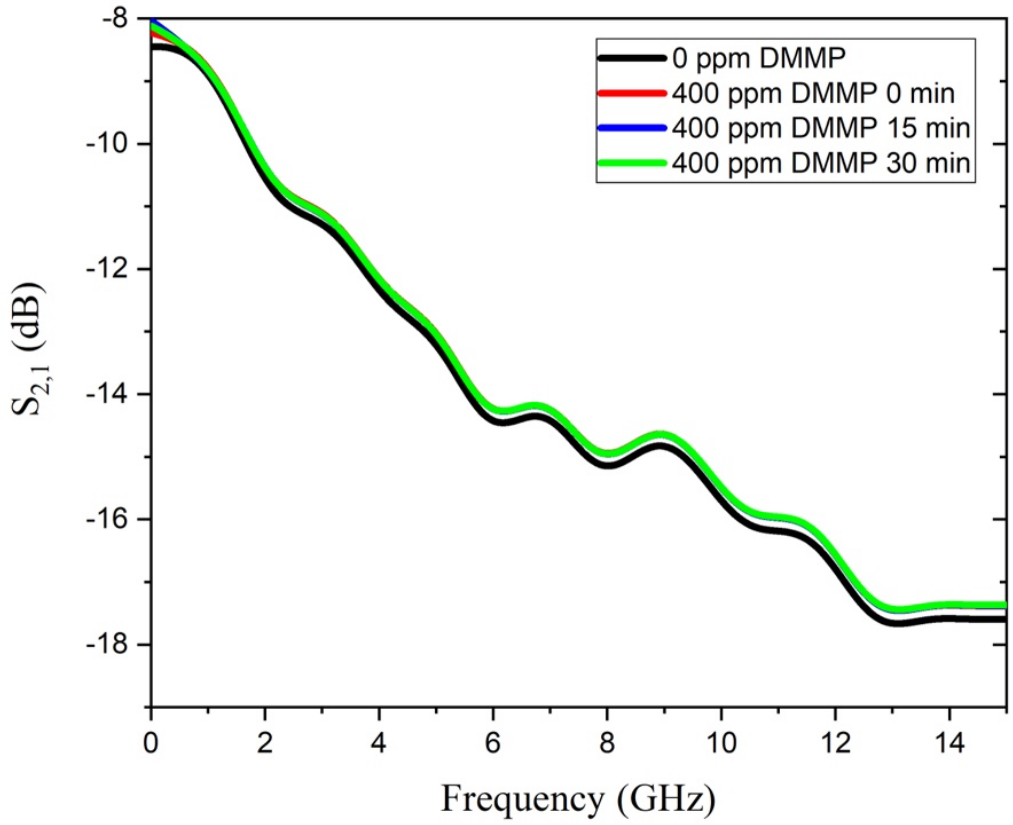

(a)

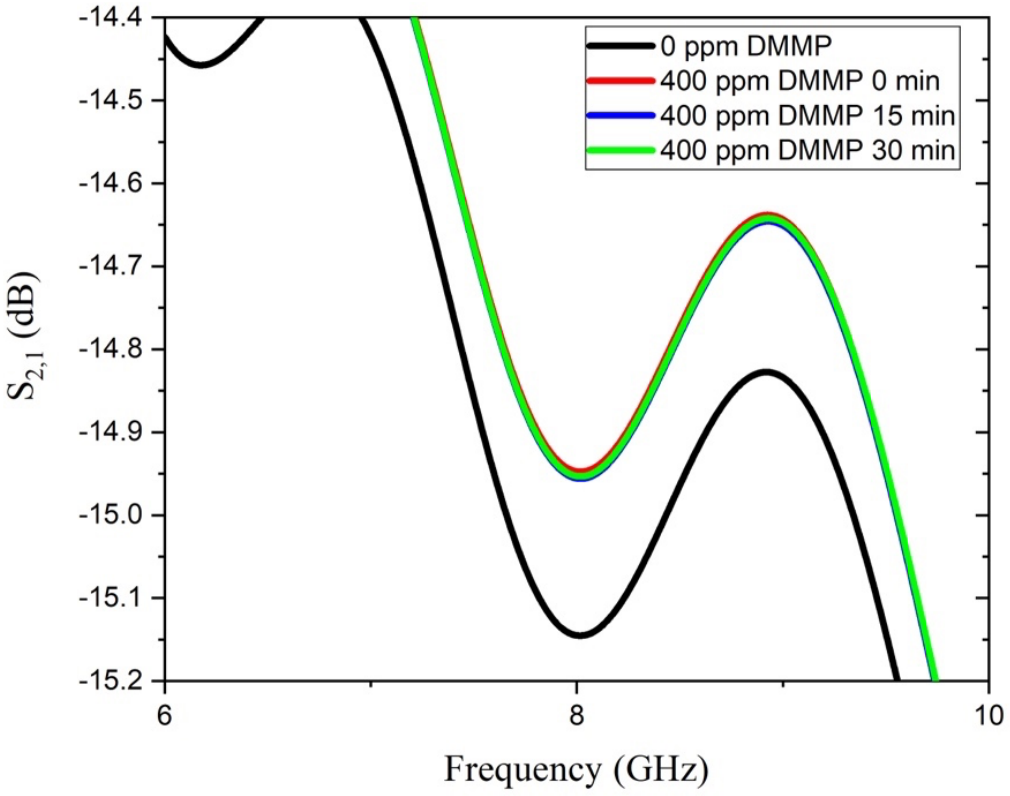

(b)
Source: The Author (2023).

When comparing the measured S_{21} responses for the sensor exposed to DMMP at different time intervals with the response in the absence of gas, a shift in the sensor response was observed. Such behavior had already been predicted by the initial simulation. Specifically, 0.2 dB decreases in the attenuation of the S_{21} response at 8 GHz were identified, indicating an increase in the conductivity of palladium.

The presented graphs indicate that the increase in palladium conductivity is instantaneous and does not show an additional variation with exposure time to DMMP gas. In other words, the sensor exhibits a two-stage behavior characteristic of an on-off type sensor. These two stages are responsible for indicating the presence (ON state) or absence (OFF state) of the gas in question.

These results reinforce the sensor's ability to detect DMMP based on the changes observed in the sensors response.

4.3.1 Increase in conductivity

After observing the increase in palladium conductivity when exposed to DMMP gas, this finding may lead to the hypothesis that in this specific case DMMP gas can donate additional electrons to the palladium layer resulting in an increase in its electrical conductivity. This process is known as chemical bonding electron donation, in which electrons from the donor atom (DMMP) transfer to the receptor atom (palladium) [75].

This transfer of additional electrons to the palladium layer can increase the electron density in the layer, which in turn increases the metal electrical conductivity. This phenomenon may have important applications in the development of new gas detection sensors, but further studies must be carried out to verify this theory.

In a situation of adsorption involving effective electron transfer, electrons from the gas are donated to the metal surface, altering the local charge on the surface. This process can lead to changes in the electronic properties and reactivity of the metallic surface [75].

Analyzing variations in both decibels and resonance frequency, it is possible to establish sensitivity parameters for the sensor. Accordingly, the sensitivity of the microwave sensor is $S_{ppm}^{|S_{21}|} = 0.0005\ dB/\%ppm$ and $S_{ppm}^{|f_{res}|} = 25\ kHz/\%ppm$

As an example of interaction between a gas and a metal, we observe the interaction between oxygen gas and copper, resulting in the formation of copper(I) oxide (Cu_2O). The study [76] provides a comparative microscopic analysis between the pure metal and its exposure to the gas as seen in Figure 25. It is evident how the gas influences the metal layer, altering factors such as particle size and, consequently, its electrical characteristics.

Figure 25 - Microscopic view of Cu metal before and after interaction with oxygen gas.

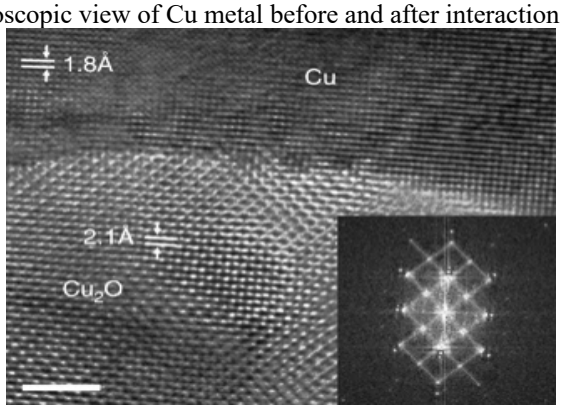

Source: Adapted From [76] (2023).

4.4 ALTERNATIVE SENSORS APPROACHES

During the PhD research period, various sensors with different metal configurations were developed for DMMP detection. Below, some of these sensors are briefly described, along with their measured results. All of them followed the same simulation methodology previously outlined, employing electromagnetic simulation software to ensure a 50-ohm line impedance.

4.4.1 Microstrip transmission line sensor with metal layers

A microstrip transmission line was tested on a quartz substrate, maintaining the same dimensions as the initially analyzed CPW sensor, including a 0.55 mm line width. In this case, with the aim of improving adhesion between palladium and quartz, metallic layers were added between palladium and the substrate, comprising a 10 nm titanium layer and a 30 nm gold layer. Additionally, palladium was assessed at a single thickness of 500 nm for sensor fabrication. The manufactured device and the S_{21} responses of the sensor when exposed to palladium gas can be seen in Figure 26.

Figure 26 - Microstrip transmission line with metal layers: a) fabricated b) measured S_{21}

(a)

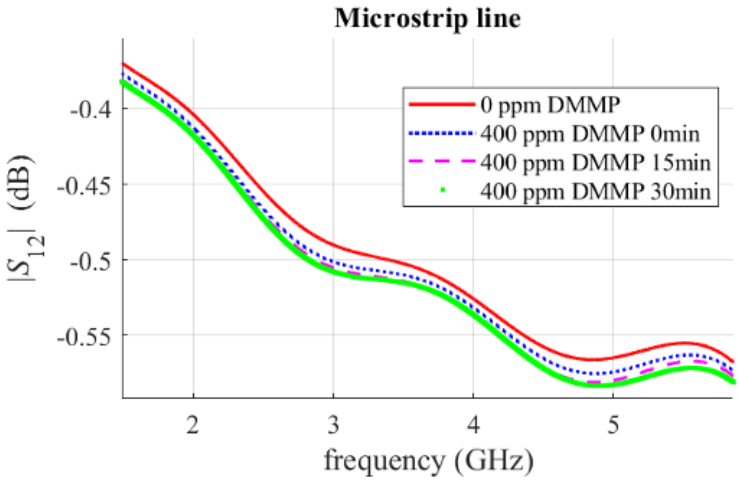

(b)

Source: The Author (2023).

Although a difference in the attenuation of the response when exposed to DMMP gas is discernible, it is apparent that the sensor displayed lower sensitivity than the CPW presented earlier in this study.

4.4.2 CPW transmission line sensor with metal layers

The concept of introducing intermediate layers, with 10 nm of titanium and 30 nm of gold, to enhance the adhesion of palladium to quartz was applied to the CPW sensor. In this context, palladium was used with a thickness of 500 nm and the sensor have the same dimensions. The system's S_{21} response is depicted in Figure 27.

Figure 27 - The S_{21} response of the CPW sensor transmission line with metal layers

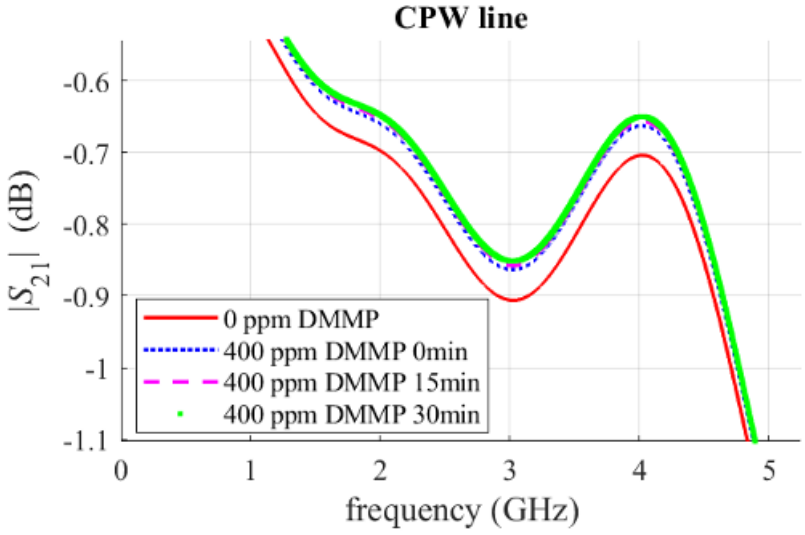

Source: The Author (2023).

It is apparent that the system demonstrated a slightly greater sensitivity compared to the microstrip under the same conditions, suggesting that the CPW system is somewhat more effective in this specific application.

4.4.3 Microstrip transmission line sensor

Finally, a microstrip transmission line sensor was tested with the same dimensions and a single 40 nm palladium layer. It shows higher sensitivity compared to sensors with metal layers but less than the initially presented sensor in this study. The manufactured device and the S_{21} responses when exposed to palladium gas can be seen in Figure 28.

Figure 28 - Microstrip transmission line: a) fabricated b) measured S_{21}

(a)

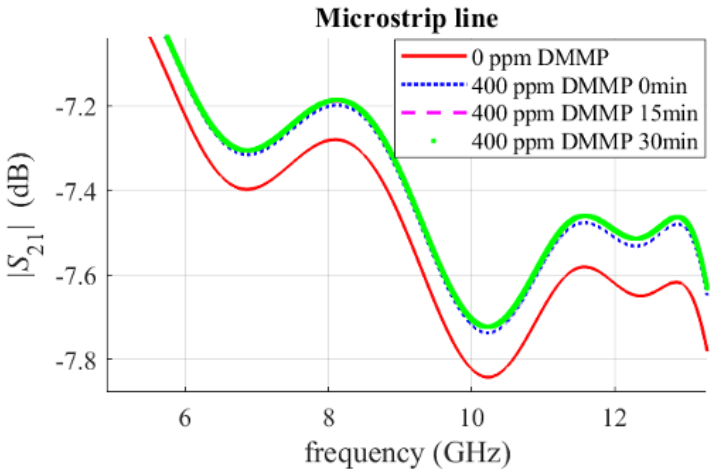

(b)

Source: The Author (2023).

5 CONCLUSION, FUTURE RESEARCH AND CONTRIBUITIONS

In this chapter, an overview of the results obtained throughout this work is presented to verify whether the proposed objectives were achieved. Based on the analysis of the results, conclusions derived from these findings will be presented. In addition, suggestions for possible future research and studies to be conducted in this area of study will be provided to improve and expand the knowledge already acquired. Two works resulting from the research conducted during the doctoral studies will also be described.

5.1 CONCLUSION

Sensors play a crucial role in detecting toxic gases and are vital for preventing and combating hazardous situations, particularly in military environments where the risk of exposure to such gases is constant. These sensors enable the early identification of harmful gases, facilitating prompt implementation of protective measures. Consequently, continuous research and development efforts are necessary to create reliable and efficient sensors capable of detecting toxic gases. Ensuring the safety and well-being of both the general population and military personnel heavily relies on the availability of such advanced sensors.

DMMP, a chemical compound utilized in the manufacturing of chemical weapons like sarin gas, serves as a representative compound for testing the efficacy of sensors in detecting warfare agents. Consequently, the investigation of sensors specifically designed to detect DMMP can contribute to the identification of other toxic gases commonly employed in military conflicts. By studying DMMP detection, valuable insights can be gained to enhance the overall capabilities of sensors in detecting a broader range of hazardous substances utilized in warfare scenarios.

CPW sensors play a vital role in the detection of toxic gases during warfare, primarily due to their exceptional sensitivity, rapid response, and selectivity. These sensors can be miniaturized, allowing for their deployment in aggressive environments and high-temperature conditions, making them highly suitable for military field applications.

In Chapter 2, an extensive examination of CPW sensor theory was undertaken, encompassing definitions, operating principles, and mathematical models. To substantiate these concepts, notable literature works showcasing the application of CPW sensors in diverse areas such as gas detection, humidity monitoring, and material permittivity measurement were

presented. This theoretical comprehension of CPW sensors plays a pivotal role in the development of the proposed sensor and its subsequent validation for the detection of DMMP gas.

In Chapter 3 of this work, the process of simulation, fabrication, and the measurement of the proposed CPW sensor is detailed. The simulation entailed the utilization of 3D electromagnetic simulation software, facilitating the selection of various physical system parameters and yielding dependable outcomes. The fabrication of the sensor involved employing specialized techniques with meticulous control over parameters, while its characterization was executed utilizing a network analyzer. The network analyzer measured the electromagnetic traits of the device under controlled circumstances, ensuring accurate assessment.

The results of the simulations and measurements were obtained and compared in chapter 4. From the analysis of the results, it was found that the computational simulation performed demonstrated accuracy in determining the attenuation of S_{21} parameter with respect to palladium thickness of 0.003 mm. However, when attempting to reproduce the same results for a thickness of 0.00004 mm (40 ηm), the software presented an error and delivered imprecise results. It is possible that this occurrence is due to the emergence of a non-local response, which is common in situations where the palladium thickness is smaller than the skin depth, and that ended up negatively impacting the accuracy of the software used for the calculations.

When analyzing the experimental results, it was found that the sensor underwent changes in its response when exposed to DMMP gas validating the theory that this gas is capable of altering the electrical conductivity of palladium. Notably, there was an increase of about 0.20 dB in the conductivity of palladium at a frequency of 8 GHz, possibly due to electron donation from the gas to the palladium.

Herein, a CPW sensor is presented that is capable of detecting DMMP gas through the analysis of its $S_{2,1}$ response. The results obtained both in simulation and measurement allowed for the observation that the presence of gas increased the electrical conductivity of the palladium layer causing a decrease in the attenuation of the response.

5.2 FUTURE RESEARCH

Due to the development of the CPW sensor for DMMP gas detection, several ideas for future work have been identified as well as the investigation of aspects that could not be fully explored:

- Performing photoelectron spectroscopy studies is a way of evaluating the hypothesis that DMMP gas increases the electrical conductivity of palladium. This technique will allow for the analysis of the interaction between the gas and the metal at the molecular level, providing a more precise and detailed approach to investigate this issue;
- To conduct further investigations on the addition of complementary metal layers to the CPW sensor, aiming to increase the sensor sensitivity to the presence of DMMP gas;
- Conduct investigations into other palladium-based structures for DMMP gas detection, not limited to planar structures, to explore sensor alternatives;
- Conduct studies for the deposition of palladium on millimeter-scale structures in a more cost-effective and efficient manner.

5.3 OTHER CONTRIBUTIONS

Throughout the years of thesis development, studies in the field of microwaves have been undertaken, with a focus on antennas, sensors, and filters. As practical outcomes of these studies, two significant works are highlighted below.

5.3.1 Non-invasive antenna for dielectric material identification at a distance

This work proposes using an antenna sensor to detect the dielectric constant of materials from a distance. Material identification involves analyzing changes in the radiation pattern or received power level when placing the material on the planar antenna sensor, as shown in Figure 29.

Figure 29 - Proposed antenna sensor concept

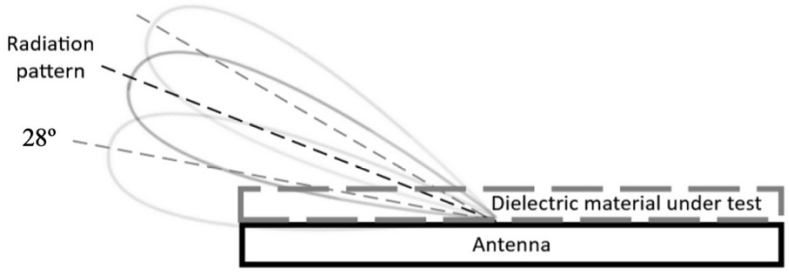

Source: The Author (2023).

The proposed antenna initially radiates at 28˚, but when a material is placed over it, there is a shift in the maximum direction of propagation. This shift in the radiation pattern enables

the non-invasive identification of the dielectric material under test by measuring received microwave signals [77]. The antenna sensor's radiation pattern points to specific angles corresponding to the material under test, allowing for distance identification without direct contact.

The proposed antenna sensor, illustrated in Figure 30, is based on the wireless communication antenna presented in [78]. This sinusoidally modulated linear surface, designed as a leaky wave antenna, features a radiation pattern depicted in Figure 30. With dimensions of 150 mm x 32 mm, it comprises 80 λ/10 elements on an Arlon© AD1000 substrate (ε_r=10.2, thickness=1.27 mm) with a small gap between adjacent metal strips. The designed operating frequency is 18 GHz, and the antenna is fed on one side by a microstrip line through an exponential transition, ensuring excellent impedance matching.

Figure 30 - Antenna sensor schematic diagram

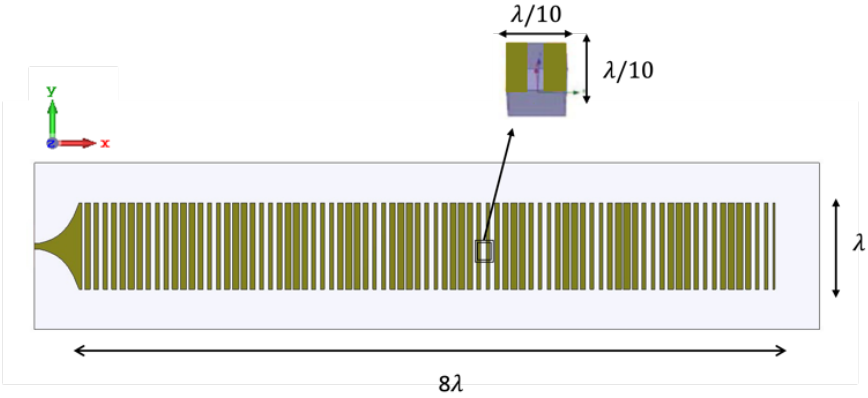

Source: Adapted From [77] (2023)

The materials under test are placed centered over the antenna sensor as shown in Figure 31.

Figure 31 - Antenna sensor with the material under test centered and placed on top

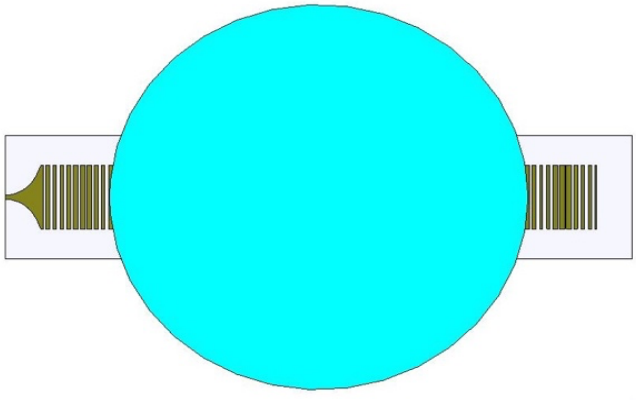

Source: The Author (2023).

The radiation diagrams presented in this work are obtained through the readout of a spectrum analyzer. The entire experimental setup, as depicted in Figure 32, is conducted within an anechoic chamber. A photograph in Figure 33 displays the experimental setup, featuring both the antenna sensor with the material under test (MUT) and the receiving horn antenna.

Figure 32 - Experimental setup schematic diagram

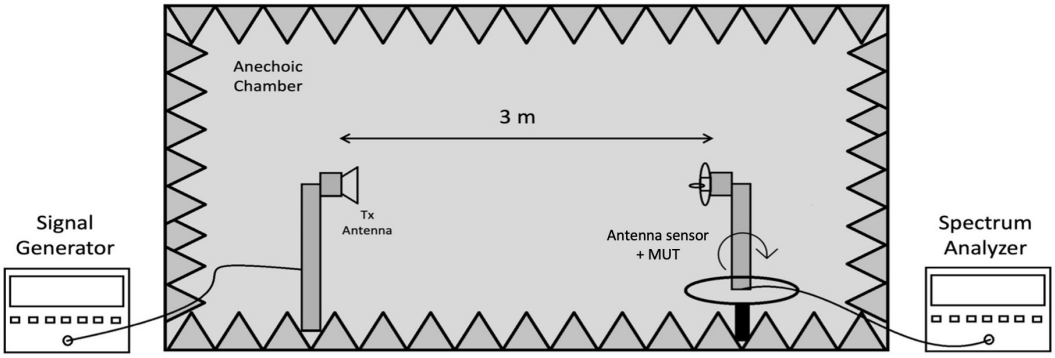

Source: The Author (2023).

Figure 33 - Proposed antenna sensor with a material under test on top

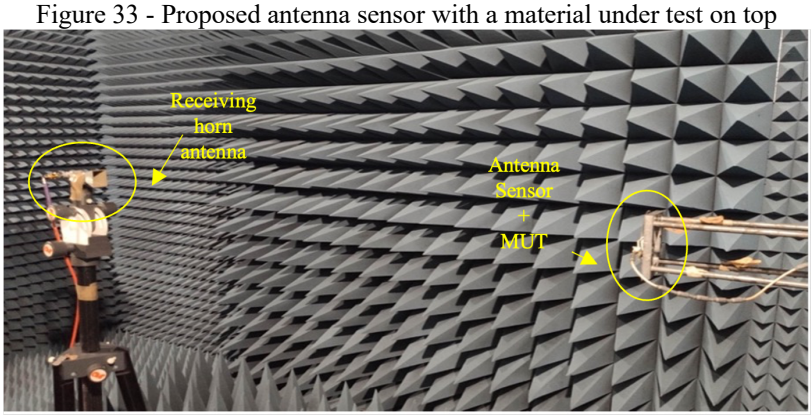

Source: The Author (2023).

In Figure 34, the simulated and measured E-plane radiation patterns of the antenna sensor at 18 GHz are shown without a material under test, with the maximum radiation occurring at 28˚. Figure 35 displays the patterns obtained for a quartz wafer under test (ε'_r: 3.75, thickness: 0.525 mm) at 18 GHz, with the maximum radiation at an angle of 33◦. The antenna's maximum radiation angle shifts from the initial θ = 28º (no material under test) to θ = 33º (with quartz). In Figure 36, the simulated and measured patterns at 18 GHz are presented for borosilicate glass (ε'_r: 4.5, thickness: 0.5 mm) as the material under test, with the maximum radiation at θ = 37º. The antenna's maximum radiation angle shifts from 28º (no material under test) to 37º (with borosilicate glass). When a low-loss material with a specific ε'_r is placed on

the antenna sensor, the maximum E-plane radiation angle shifts, enabling non-invasive material identification at a distance.

Figure 34 - Simulated and measured radiation patterns of the antenna sensor at 18 GHz (without material under test)

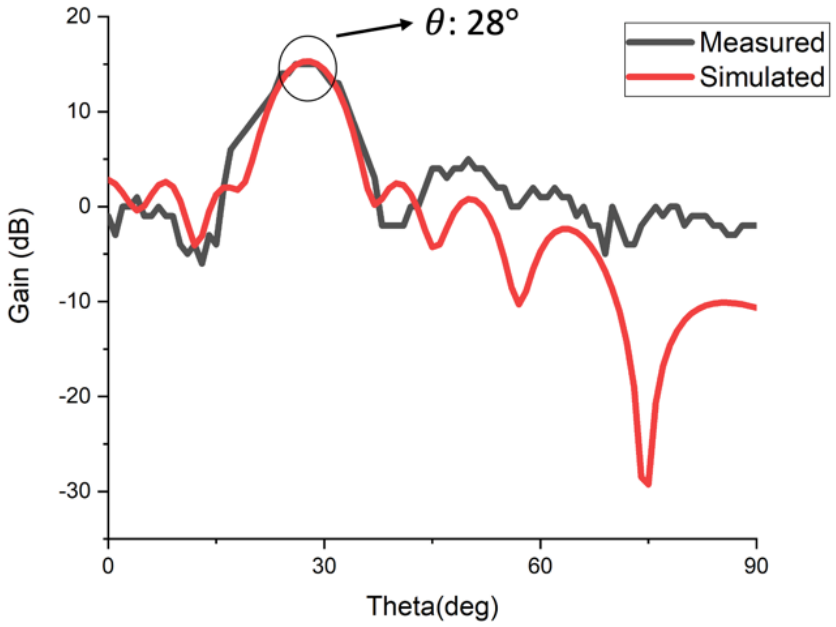

Source: The Author (2023).

Figure 35 - Radiation pattern of the antenna sensor with quartz wafer under test above

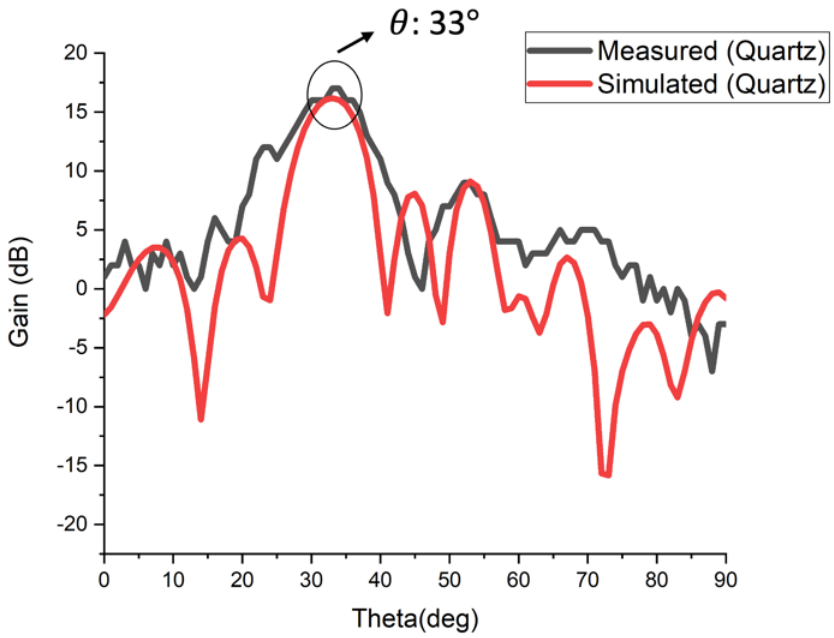

Source: The Author (2023).

Figure 36 - Radiation pattern of the antenna sensor with a borosilicate glass wafer under test on top

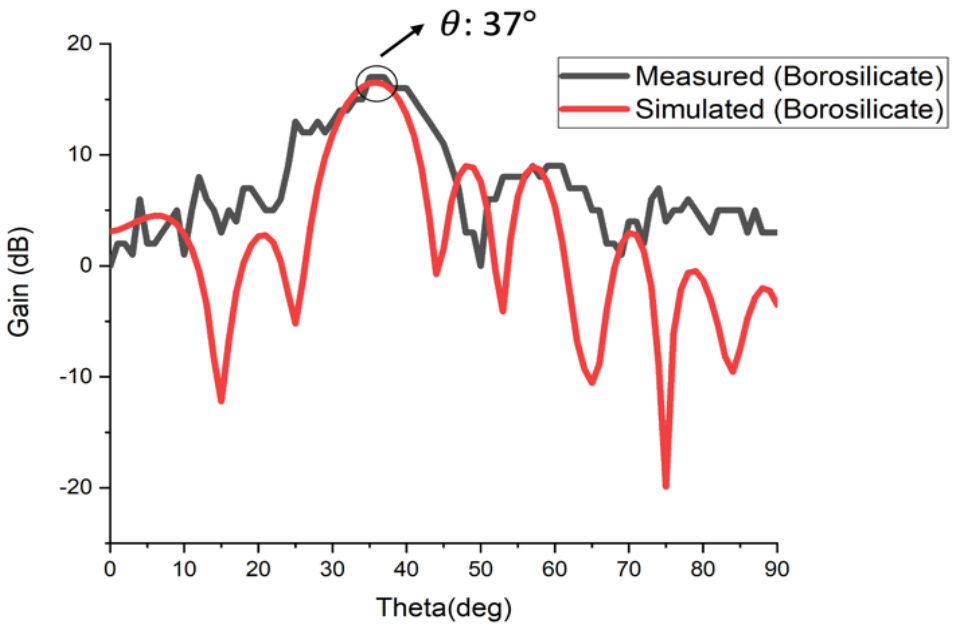

Source: The Author (2023).

5.3.2 Waveguide Filter for Instantaneous Frequency Measurement Systems

This work presents a new 3D configuration for an IFM system filter designed to operate in a range frequency from 15 GHz to 15.16 GHz. The filters can identify up to four intervals characterized by unknown frequencies.

Two waveguide filters for a 2-bit IFM system are introduced, inspired by microstrip filters from [79]. Rectangular resonant cavities, connected to the waveguide through irises, resonate at different frequencies. The design focuses on achieving the desired frequency response, as illustrated in Figure 37. Electromagnetic simulation software was used to perform simulations.

Figure 37 - Characteristic response of the 2-bit IFM system

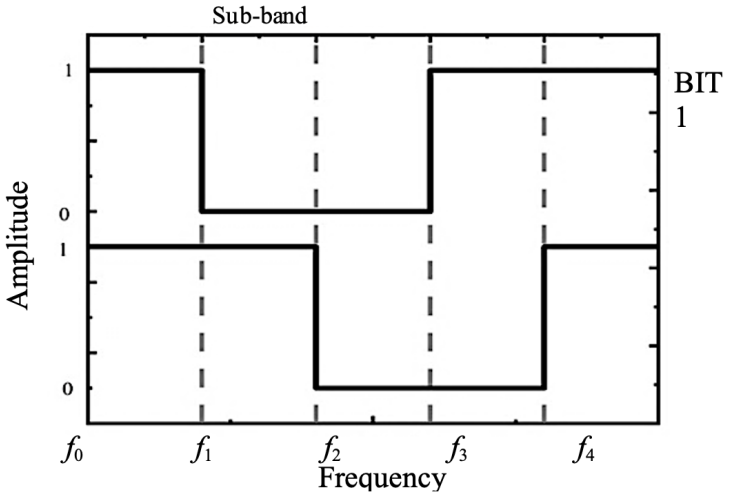

1	0	0	1	BIT 1
1	1	0	0	BIT 0
1	2	3	4	Sub-band

Source: The Author (2023).

The filter in Figure 38 consists of a waveguide and a resonant cavity connected by a 1 mm thick iris with width di and length *d*r. It functions as a narrowband reject filter. Figure 39 illustrates the typical frequency response of the filter with a resonator for four different *d*r values. The filter displays a bandwidth of approximately 0.4% at the resonance frequency (for *d*i = 8 mm and h = 6 mm). The resonance frequency is determined by the length *d*r and exhibits an almost linear and inversely proportional relationship to it.

Figure 38 - Filter with one resonant cavity; a = 15.8 mm, b = 7.9 mm

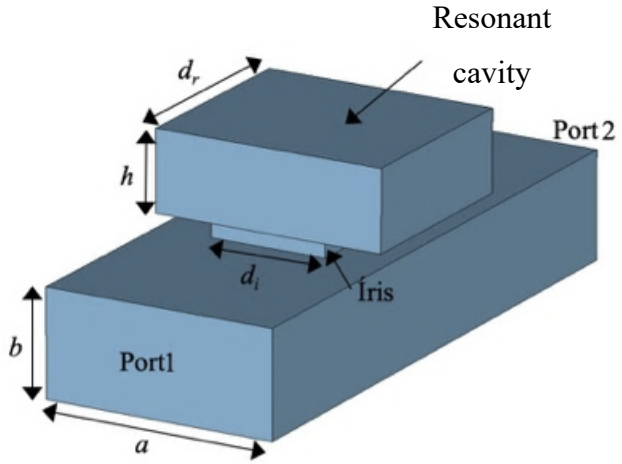

Source: The Author (2023).

Figure 39 - Simulation results for a variable resonant cavity in a waveguide connection; dr1 = 13.99 mm, dr2 = 13.92 mm, dr3 = 13.85 mm, dr4 = 13.76

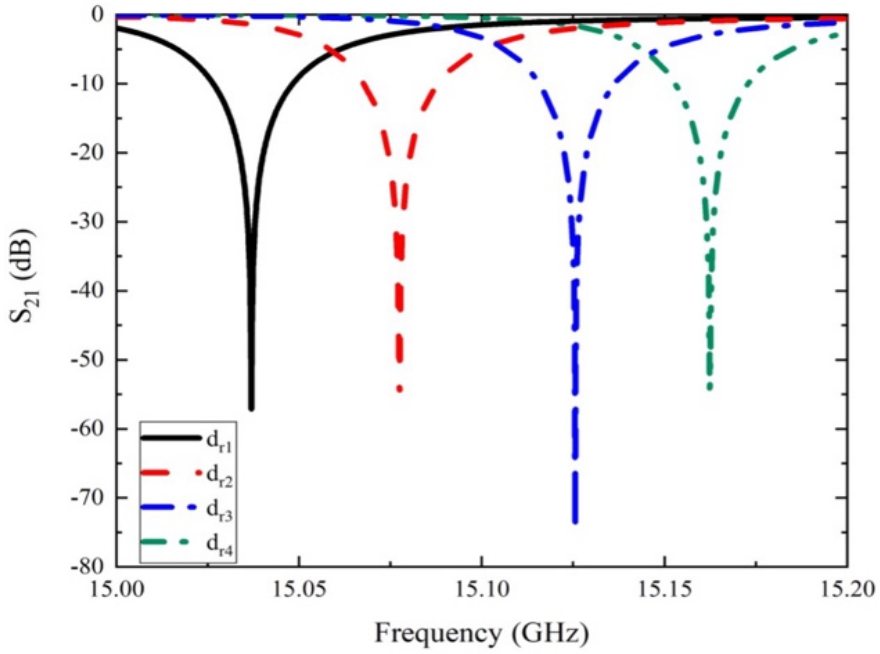

Source: The Author (2023).

The proposed 2-bit IFM system, operating between 15 and 15.17 GHz, identifies signals in four sub-bands of approximately 43 MHz each using two filters. Each filter consists of an 80 mm waveguide and three resonators, as depicted in Figure 40.

Figure 40 - Waveguide filter with three resonant cavities

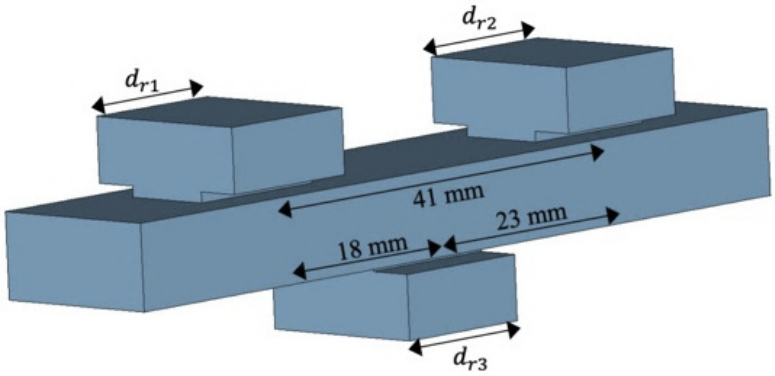

Source: The Author (2023).

In the first filter (BIT 1), resonators are tuned to 15.04 GHz (f_1) (d_r = 13.99 mm), 15.8 GHz (f_2) (d_r = 13.92 mm), and 15.12 GHz (f_3) (d_r = 13.85 mm), while in the second filter (BIT 0), resonators are set for 15.08 GHz (f_1) (d_r = 13.92 mm), 15.12 GHz (f_2) (d_r = 13.85 mm), and 15.16 GHz (f_3) (d_r = 13.76 mm). Resonators on the same transmission line experience mutual interference in their resonance frequencies, with optimized distances between resonators ($d_{1,2}$ = 41 mm, $d_{1,3}$ = 18 mm, and $d_{2,3}$ = 23 mm). The total bandwidth of each filter is the sum of individual resonator bandwidths, illustrated in Figure 41 and Figure 42.

Figure 41 - Simulation results of the filter for BIT 1 (solid line) and the resonant cavities

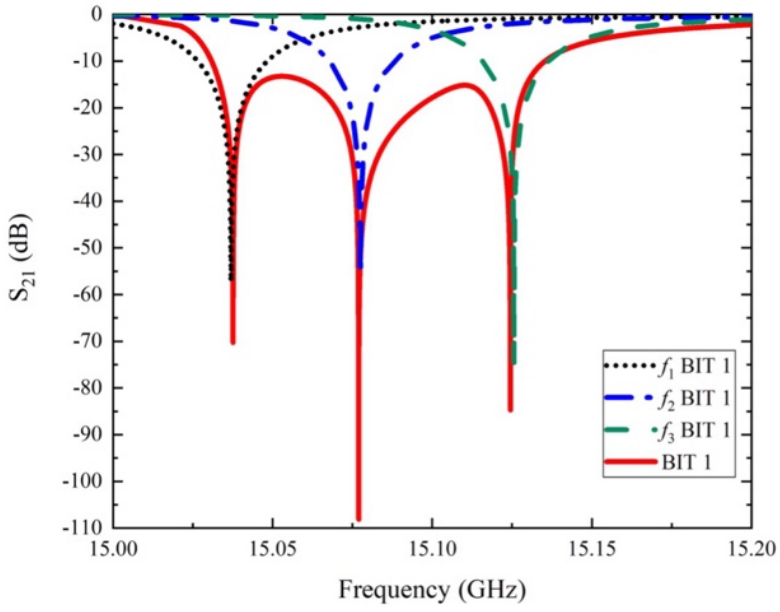

Source: The Author (2023).

Figure 42 - Simulation results of the filter for BIT 0 (solid line) and the resonant cavities

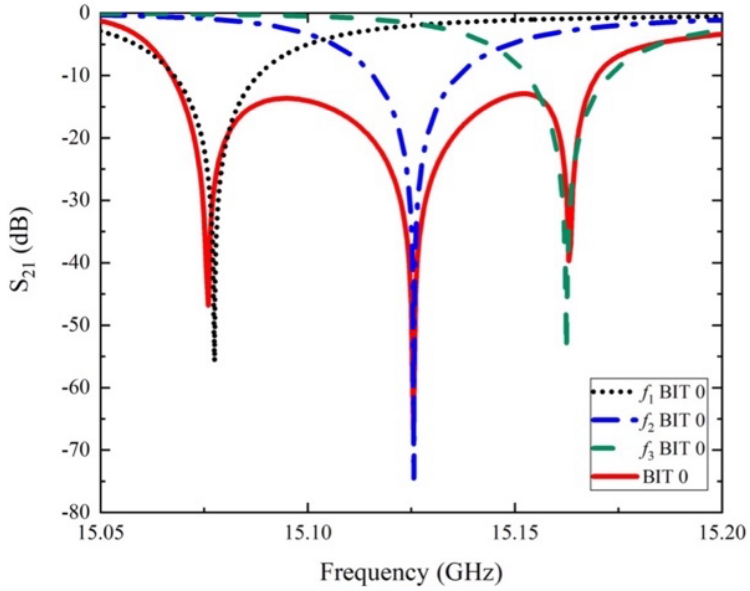

Source: The Author (2023).

Figure 43 shows simulation results for BIT 0 and 1, with binary sequences generated under a -10 dB threshold level (*Blevel*) for both filters. The filters provide BIT 0 for $|S_{21}|$ below -10 dB and BIT 1 for $|S_{21}|$ above -10 dB. The system identifies signals in four distinct sub-bands, each with an average width of 43 MHz. Binary sequence: 11 (15 – 15.038 GHz), 01 (15.038 – 15.075 GHz), 00 (15.075 – 15.13 GHz) and 10 (15.13 – 15.17 GHz).

Figure 43 - Simulation results of the filters for BIT 1 (solid line) and BIT 0 (dot line)

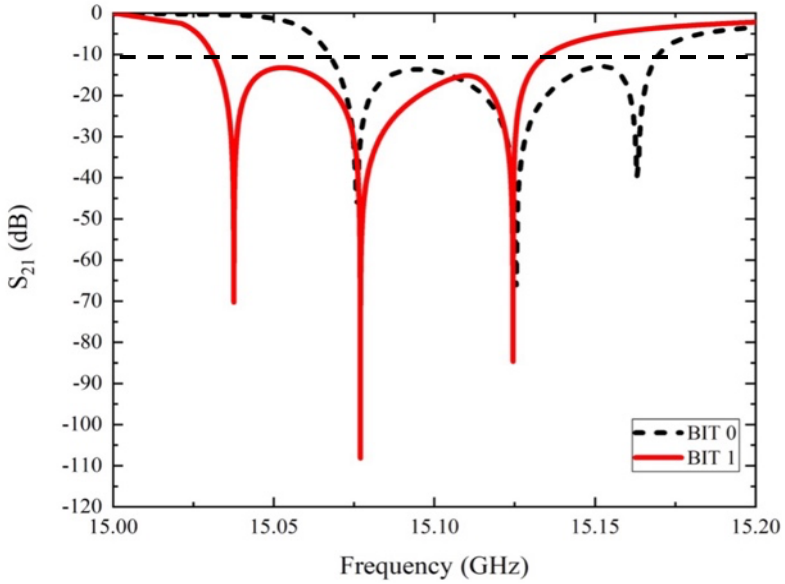

Source: The Author (2023).

The waveguide filters were designed using 3D electromagnetic simulation software, followed by manufacturing and measurement using a vector network analyzer (VNA). The fabricated prototype is shown in Figure 44.

Figure 44 - Manufactured waveguide filter: (a) BIT 0 and (b) BIT 0 with connectors

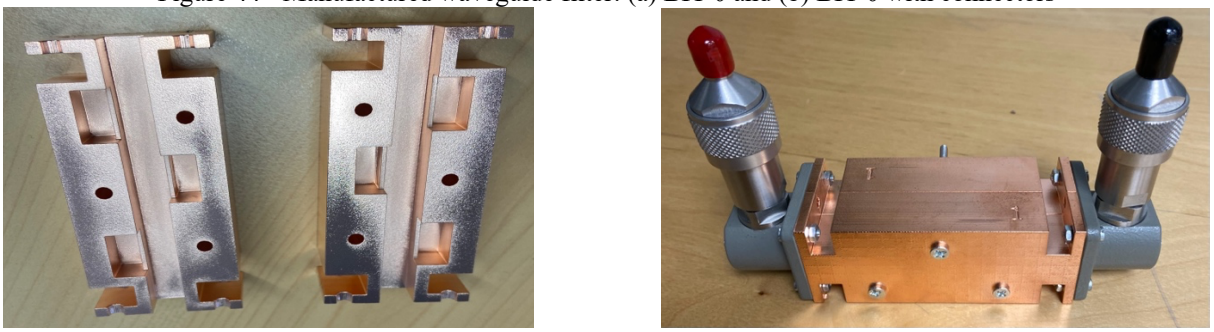

(a) (b)

Source: The Author (2023).

Each waveguide filter, assembled in two parts, was manufactured and measured for BIT 0. The measurements closely aligned with simulations, confirming the concept and maintaining the system's frequency ranges, as seen in Figure 45.

Figure 45 - Comparison between simulated and measured S_{21} for BIT 0

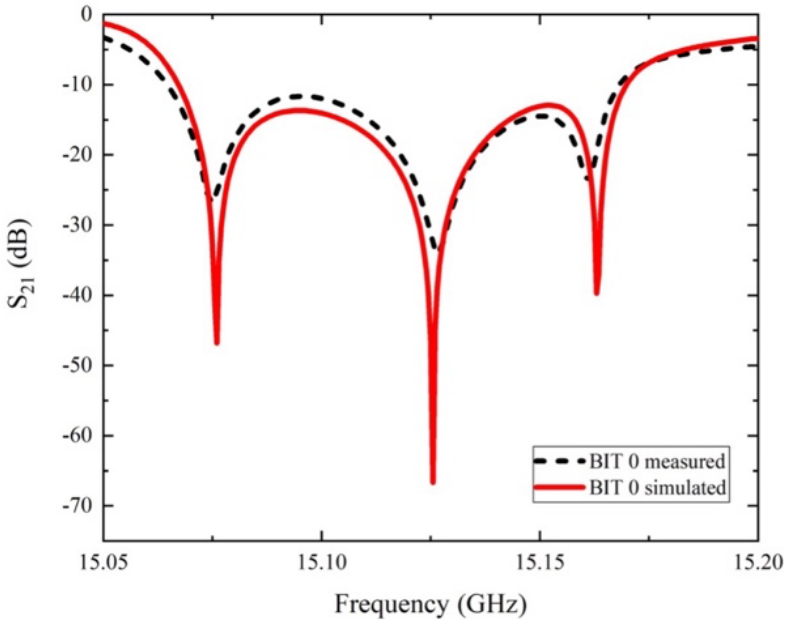

Source: The Author (2023).

In BIT 1 system measurements, a compressed response was observed, likely due to resonator coupling not considered in the simplified simulation model. This absence led to

mutual interference between resonators, increasing electromagnetic losses and resulting in a compressed measured response, as shown in Figure 46.

Figure 46 - Comparison between simulated and measured S_{21} for BIT 1

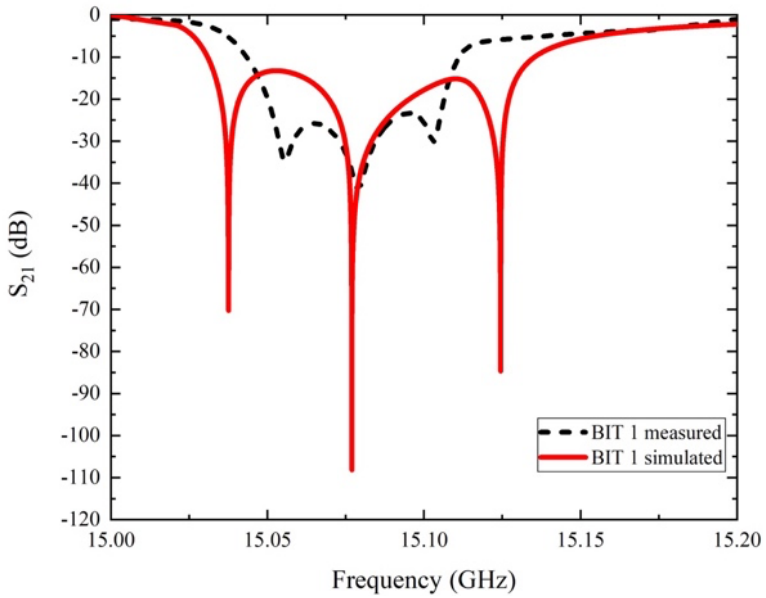

Source: The Author (2023).

5.4 CONTRIBUTIONS AND SCIENTIFIC PRODUCTION

As a testament to the contributions resulting from the studies conducted throughout this PhD, the outcomes presented in this thesis have led to the development of a collection of scientific publications. These results were achieved either directly or through collaborative efforts within UFPE's LabMicro.

5.4.1 Papers published in journals

a) J. A. I. Araujo, I. Llamas-Garro, Z. Brito-Brito, F. Mira, X. Artiga, and M. T. de Melo, "Non-invasive antenna sensor for dielectric material identification at a distance," *Measurement*, vol. 224, p. 113842, Jan. 2024, doi: 10.1016/j.measurement.2023.113842.

b) J. A. I. Araujo *et al.*, "Reconfigurable Filtenna using Varactor Diode for Wireless Applications," *Journal of Microwaves, Optoelectronics and Electromagnetic Applications*, vol. 20, no. 4, pp. 834–854, Dec. 2021, doi: 10.1590/2179-10742021v20i4115.

c) P. H. B. Cavalcanti Filho *et al.*, "Planar Sensor for Material Characterization Based on the Sierpinski Fractal Curve," *J Sens*, vol. 2020, pp. 1–9, Dec. 2020, doi: 10.1155/2020/8830596.

d) C. P. do N. Silva, J. A. I. Araujo, M. S. Coutinho, M. R. T. de Oliveira, I. Llamas-Garro, and M. T. de Melo, “Multi-band microwave sensor based on Hilbert’s fractal for dielectric solid material characterization,” *J Electromagn Waves Appl*, vol. 35, no. 7, pp. 848–860, May 2021, doi: 10.1080/09205071.2020.1861992.

5.4.2 Papers published in conference editorials

a) J. A. I. Araujo *et al.*, “Analysis of a microwave filter parameters for design optimization via machine learning,” in *IMOC 2023*, Castelldefels: SBMO/ IEEE MTT-S, Nov. 2023.

b) P. H. B. Cavalcanti Filho, M. O. Alencar, E. M. F. Oliveira, A. G. Barboza, J. A. I. Araujo, and M. T. de Melo, “4-BIT FSS Based IFM System Using Balanced Binary Code,” in *IMOC 2023*, Castelldefels: SBMO/IEEE MTT-S, Nov. 2023.

c) C. P. do N. Silva, J. A. I. Araujo, I. Llamas-Garro, and M. T. de Melo, “Filtro em Guia de Onda para Sistemas de Medição Instantânea de Frequências,” in *MOMAG 2020. Anais do MOMAG 2020*, São Caetano do Sul: SBMO, Nov. 2020, pp. 201–204.

d) F. A. C. S. Lucena *et al.*, “A New Trapezium FSS Superstrate for Antenna Gain Enhancement,” in *2019 SBMO/IEEE MTT-S International Microwave and Optoelectronics Conference (IMOC)*, IEEE, Nov. 2019, pp. 1–3. doi: 10.1109/IMOC43827.2019.9317589.

e) P. H. B. Cavalcanti Filho, J. A. I. Araujo, M. R. T. de Oliveira, M. T. de Melo, A. G. Neto, and I. B. G. Coutinho, “A New Design of Sierpinski Curve Fractal FSS for S-band Interference Protection Applications,” in *2019 SBMO/IEEE MTT-S International Microwave and Optoelectronics Conference (IMOC)*, IEEE, Nov. 2019, pp. 1–3. doi: 10.1109/IMOC43827.2019.9317417.

REFERENCES

[1] SIDELL, F. R.; BORAK, J. Chemical warfare agents: II. nerve agents. **Annals of Emergency Medicine**, jul. 1992. v. 21, n. 7, p. 865–871.

[2] GUPTA, R. D. *et al.* Directed evolution of hydrolases for prevention of G-type nerve agent intoxication. **Nature Chemical Biology**, 9 fev. 2011. v. 7, n. 2, p. 120–125.

[3] SUZUKI, T. *et al.* Sarin poisoning in Tokyo subway. **Lancet (London, England)**, 15 abr. 1995. v. 345, n. 8955, p. 980.

[4] POWROŹNIK, P.; JAKUBIK, W.; KAŹMIERCZAK-BAŁATA, A. Detection of Organophosphorus (DMMP) Vapour Using Phthalocyanine-palladium Bilayer Structures. **Procedia Engineering**, 2015a. v. 120, p. 368–371.

[5] HARTMANN-THOMPSON, C.; KEELEY, D. L.; GALLAGHER, S. Hydrogen-bond basic siloxane phosphonate polymers for surface acoustic wave (SAW) sensors. **Sensors and Actuators B: Chemical**, jun. 2006. v. 115, n. 2, p. 697–699.

[6] ORDRONNEAU, L. *et al.* Chromogenic detection of Sarin by discolouring decomplexation of a metal coordination complex. **Chemical Communications**, 2013. v. 49, n. 79, p. 8946.

[7] RUSU, A. D. *et al.* Fluorescent polymeric aggregates for selective response to Sarin surrogates. **Chem. Commun.**, 2014. v. 50, n. 69, p. 9965–9968.

[8] DAI, Z. *et al.* Janus gas: reversible redox transition of Sarin enables its selective detection by an ethanol modified nanoporous SnO_2 chemiresistor. **Chemical Communications**, 2015. v. 51, n. 38, p. 8193–8196.

[9] BARBA-BON, A. *et al.* Chromo-fluorogenic BODIPY-complexes for selective detection of V-type nerve agent surrogates. **Chem. Commun.**, 10 set. 2014. v. 50, n. 87, p. 13289–13291.

[10] SKULSKI, J.; GALWAS, B. A. Planar resonator sensor for moisture measurements. [S.l.]: **Telecommun. Res. Inst**, [s.d.]. p. 692–695.

[11] GALWAS, B. A.; PIOTROWSKI, J. K.; SKULSKI, J. Dielectric measurements using a coaxial resonator opened to a waveguide below cut-off. **IEEE Transactions on Instrumentation and Measurement**, abr. 1997. v. 46, n. 2, p. 511–514.

[12] GALWAS, B. A.; PIOTROWSKI, J. K.; SKULSKI, J. New type of microwave resonator sensors with waveguide below cut-off. [S.l.]: IEEE, 1996. p. 76–77.

[13] YEOW, Y. K. *et al.* Application of bandpass filter as a sensor for rice characterization. [S.l.]: IEEE, 2010. p. 570–573.

[14] SABBAGH, M. A. EL *et al.* Use of microstrip patch antennas in grain permittivity measurement. [S.l.]: IEEE, 2003. p. 640–644.

[15] FERICEAN, S. *et al.* Development of a microwave proximity sensor for industrial applications. [S.l.]: IEEE, 2008. p. 1402–1405.

[16] KOROSTYNSKA, O.; MASON, A.; AL-SHAMMA'A, A. Microwave sensors for the non-invasive monitoring of industrial and medical applications. **Sensor Review**, 17 mar. 2014. v. 34, n. 2, p. 182–191.

[17] GRAMMER, W.; YNGVESSON, K. S. Coplanar waveguide transitions to slotline: design and microprobe characterization. **IEEE Transactions on Microwave Theory and Techniques**, 1993. v. 41, n. 9, p. 1653–1658.

[18] BOGNER, A. *et al.* Planar Microstrip Ring Resonators for Microwave-Based Gas Sensing: Design Aspects and Initial Transducers for Humidity and Ammonia Sensing. **Sensors**, 24 out. 2017. v. 17, n. 10, p. 2422.

[19] CHEN, L. F. *et al.* **Microwave Electronics**. [S.l.]: Wiley, 2004.

[20] SILVA DOS SANTOS, K. *et al.* Hybrid Microstrip Device for Hydrogen Detection at Microwave Frequencies. **IEEE Sensors Journal**, 1 abr. 2023. v. 23, n. 7, p. 6810–6821.

[21] BAROCHI, G.; ROSSIGNOL, Jérôme; BOUVET, M. Development of microwave gas sensors. **Sensors and Actuators B: Chemical**, out. 2011. v. 157, n. 2, p. 374–379.

[22] KIM, B.-H. *et al.* A gas sensor using double split-ring resonator coated with conducting polymer at microwave frequncies. [S.l.]: IEEE, 2014. p. 1815–1818.

[23] ALOISIO, D.; DONATO, N. Development of Gas Sensors on Microstrip Disk Resonators. **Procedia Engineering**, 2014. v. 87, p. 1083–1086.

[24] JOUHANNAUD, J.; ROSSIGNOL, J; STUERGA, D. Metal oxide-based gas sensor and microwave broad-band measurements: an innovative approach to gas sensing. **Journal of Physics: Conference Series**, 1 jul. 2007. v. 76, p. 012043.

[25] BAILLY, G. *et al.* Influence of the Design in Microwave-based Gas Sensors: Ammonia Detection with Titania Nanoparticles. **Procedia Engineering**, 2016. v. 168, p. 264–267.

[26] WU, B. *et al.* High-Performance Wireless Ammonia Gas Sensors Based on Reduced Graphene Oxide and Nano-Silver Ink Hybrid Material Loaded on a Patch Antenna. **Sensors**, 9 set. 2017. v. 17, n. 9, p. 2070.

[27] BAILLY, Guillaume *et al.* Microstrip Spiral Resonator For Microwave-Based Gas Sensing. **IEEE Sensors Letters**, ago. 2017. v. 1, n. 4, p. 1–4.

[28] SOROCKI, J.; RYDOSZ, A.; STASZEK, K. Wideband microwave multiport-based system for low gas concentration sensing and its application for acetone detection. **Sensors and Actuators B: Chemical**, nov. 2020. v. 323, p. 128710.

[29] KRUDPUN, W. *et al.* PSE-Coated Interdigital Resonator for Selective Detection of Ammonia Gas Sensor. **IEEE Sensors Journal**, 1 dez. 2019. v. 19, n. 23, p. 11228–11235.

[30] RIAD, M. M. Y. R.; ELDAMAK, A. R. Coplanar Waveguide Based Sensor Using Paper Superstrate for Non-Invasive Sweat Monitoring. **IEEE Access**, 2020. v. 8, p. 177757–177766.

[31] SILVA, C. P. Do N. **Interferômetro E Sensor Multibanda Baseados Na Curva Fractal De Hilbert**. Recife: Universidade Federal de Pernambuco, 2020. PhD Thesis.

[32] WEN, C. P. Coplanar Waveguide, a Surface Strip Transmission Line Suitable for Nonreciprocal Gyromagnetic Device Applications. [S.l.]: IEEE, 1969. p. 110–115.

[33] MARTÍN, F. Metamaterials for Wireless Communications, Radiofrequency Identification, and Sensors. **ISRN Electronics**, 20 dez. 2012. v. 2012, p. 1–29.

[34] GHIONE, G.; NALDI, C. U. Coplanar Waveguides for MMIC Applications: Effect of Upper Shielding, Conductor Backing, Finite-Extent Ground Planes, and Line-to-Line Coupling. **IEEE Transactions on Microwave Theory and Techniques**, mar. 1987. v. 35, n. 3, p. 260–267.

[35] GARCÍA BAÑOS, B. **Estudio y optimización de sensores de microondas para la caracterización y monitorización de materiales en procesos industriales.** Valencia (Spain): Universitat Politècnica de València, 2008.

[36] SAMANT, H. *et al.* Design of CPW fed IDC resonator for non invasive testing of chemical solvents. [S.l.]: IEEE, 2015. p. 1–4.

[37] TIWARI, N. K.; SINGH, S. P.; AKHTAR, M Jaleel. Coplanar waveguide based planar RF sensor for the detection of adulteration in oils. [S.l.]: IEEE, 2017. p. 1–2.

[38] EYEBE, G. A. *et al.* Fully printed CPW-based microwave humidity sensor in phase shifting paradigm. [S.l.]: IEEE, 2019. p. 1–3.

[39] JINGJING; ALEXANDROU, S.; HSIANG, T. Y. Attenuation characteristics of coplanar waveguides at subterahertz frequencies. **IEEE Transactions on Microwave Theory and Techniques**, nov. 2005. v. 53, n. 11, p. 3281–3287.

[40] SIMONS, R. N. **Coplanar Waveguide Circuits, Components, and Systems**. [S.l.]: Wiley, 2001.

[41] TSUJI, M.; SHIGESAWA, H.; OLINER, A. A. New interesting leakage behavior on coplanar waveguides of finite and infinite widths. **IEEE Transactions on Microwave Theory and Techniques**, 1991. v. 39, n. 12, p. 2130–2137.

[42] EDWARDS, T. C.; STEER, M. B. **Foundations of Interconnect and Microstrip Design**. [S.l.]: Wiley, 2000.

[43] GARG, R.; BAHL, I.; BOZZI, M. **Microstrip Lines and Slotlines**. 3. ed. [S.l.]: Artech House, 2013.

[44] GHIONE, G.; NALDI, C. Analytical formulas for coplanar lines in hybrid and monolithic MICs. **Electronics Letters**, 1984. v. 20, n. 4, p. 179.

[45] GARCÍA, P. J. **Evaluación no destructiva de estructuras de obra civil mediante métodos electromagnéticos**. Barcelona: Universitat Politècnica de Catalunya, 2011. PhD Thesis.

[46] WEN, C. P. Attenuation characteristics of coplanar waveguides. **Proceedings of the IEEE**, 1970. v. 58, n. 1, p. 141–142.

[47] HILBERG, W. From Approximations to Exact Relations for Characteristic Impedances. **IEEE Transactions on Microwave Theory and Techniques**, maio. 1969. v. 17, n. 5, p. 259–265.

[48] POZAR, D. M. **Microwave Engineering**. 4. ed. [S.l.]: John Wiley & Sons, 2011.

[49] BRUNOL, E. *et al.* Detection of dimethyl methylphosphonate (DMMP) by tin dioxide-based gas sensor: Response curve and understanding of the reactional mechanism. **Sensors and Actuators B: Chemical**, dez. 2006. v. 120, n. 1, p. 35–41.

[50] BARTELT-HUNT, S. L.; KNAPPE, D. R. U.; BARLAZ, M. A. A Review of Chemical Warfare Agent Simulants for the Study of Environmental Behavior. **Critical Reviews in Environmental Science and Technology**, 18 jan. 2008. v. 38, n. 2, p. 112–136.

[51] MUKHOPADHYAY, S.; SCHOENITZ, M.; DREIZIN, E. L. Vapor-phase decomposition of dimethyl methylphosphonate (DMMP), a sarin surrogate, in presence of metal oxides. **Defence Technology**, ago. 2021. v. 17, n. 4, p. 1095–1114.

[52] POWROŹNIK, P.; JAKUBIK, W.; KAŹMIERCZAK-BAŁATA, A. Detection of Organophosphorus (DMMP) Vapour Using Phthalocyanine-palladium Bilayer Structures. **Procedia Engineering**, 2015a. v. 120, p. 368–371.

[53] REY, E. *et al.* The semiconductivity and stability of palladium oxide. **Journal of Materials Science**, abr. 1978. v. 13, n. 4, p. 812–816.

[54] NINNO, A. DE; GIUDICE, E. DEL; FRATTOLILLO, A. Excess Heat and Calorimetric Calculation: Evidence of Coherent Nuclear Reactions in Condensed Matter at Room Temperature. [S.l.]: [s.n.], 2008, p. 127–152.

[55] WILLIAMS, D. E. Semiconducting oxides as gas-sensitive resistors. **Sensors and Actuators B: Chemical**, set. 1999. v. 57, n. 1–3, p. 1–16.

[56] POWROŹNIK, P.; JAKUBIK, W.; KAŹMIERCZAK-BAŁATA, A. Detection of Organophosphorus (DMMP) Vapour Using Phthalocyanine-palladium Bilayer Structures. **Procedia Engineering**, 2015a. v. 120, p. 368–371.

[57] LIU, J. (Jimmy). Advanced Electron Microscopy of Metal–Support Interactions in Supported Metal Catalysts. **ChemCatChem**, 14 jun. 2011. v. 3, n. 6, p. 934–948.

[58] RANA, L. *et al.* ZnO/ST-Quartz SAW resonator: An efficient NO2 gas sensor. **Sensors and Actuators B: Chemical**, nov. 2017. v. 252, p. 840–845.

[59] AL-SALMAN, H. S.; ABDULLAH, M. J. Hydrogen gas sensing based on ZnO nanostructure prepared by RF-sputtering on quartz and PET substrates. **Sensors and Actuators B: Chemical**, maio. 2013. v. 181, p. 259–266.

[60] ALANAZI, N.; ALMUTAIRI, M.; ALODHAYB, A. N. A Review of Quartz Crystal Microbalance for Chemical and Biological Sensing Applications. **Sensing and Imaging**, 4 mar. 2023. v. 24, n. 1, p. 10.

[61] REYES, A. C. *et al.* Coplanar waveguides and microwave inductors on silicon substrates. **IEEE Transactions on Microwave Theory and Techniques**, 1995. v. 43, n. 9, p. 2016–2022.

[62] **3680 Series Universal Test Fixture Operation and Maintenance Manual**. [S.l.]: [s.n.], 2022.

[63] JAIN, P. C.; KUSHWAHA, R. Wireless gas sensor network for detection and monitoring of harmful gases in utility areas and industries. [S.l.]: IEEE, 2012. p. 642–646.

[64] MUNTEANU, I.; HANNINEN, I. Recent advances in CST STUDIO SUITE for antenna simulation. [S.l.]: IEEE, 2012. p. 1301–1305.

[65] SAHU, N.; PARIJA, B.; PANIGRAHI, S. Fundamental understanding and modeling of spin coating process: A review. **Indian Journal of Physics**, 12 abr. 2009. v. 83, n. 4, p. 493–502.

[66] MEI, D. *et al.* A High Resolution Spatial Smoothing Algorithm. [S.l.]: IEEE, 2007. p. 1031–1034.

[67] CHEN, C.-J.; SUNG, C.-H.; SU, Y.-D. A Multi-Stub Lowpass Filter. **IEEE Microwave and Wireless Components Letters**, ago. 2015. v. 25, n. 8, p. 532–534.

[68] VALKENBURG, M. E. VAN; MIDDLETON, W. M. **Reference Data for Engineers: Radio, Electronics, Computers and Communications**. 9. ed. [S.l.]: Newnes, 2011.

[69] ABEDEEN, Z.; AGARWAL, P. Microwave sensing technique-based label-free and real-time planar glucose analyzer fabricated on FR4. **Sensors and Actuators A: Physical**, ago. 2018. v. 279, p. 132–139.

[70] KRUPKA, J. Frequency domain complex permittivity measurements at microwave frequencies. **Measurement Science and Technology**, 1 jun. 2006. v. 17, n. 6, p. R55–R70.

[71] COLLIER, R.; SKINNER, D. **Microwave Measurements**. 3. ed. [S.l.]: IET, 2007.

[72] ALAHNOMI, R. A. *et al.* Review of Recent Microwave Planar Resonator-Based Sensors: Techniques of Complex Permittivity Extraction, Applications, Open Challenges and Future Research Directions. **Sensors**, 24 mar. 2021. v. 21, n. 7, p. 2267.

[73] LAGARKOV, A. N.; VINOGRADOV, A. P. Non-Local Response of Composite Materials in Microwave Range. **Advances in Complex Electromagnetic Materials**. Dordrecht: Springer Netherlands, 1997, p. 117–130.

[74] JAVADZADEH, S. M. H.; FARZANEH, F.; FARDMANESH, M. Analytical distributed non-linear model for symmetric and asymmetric superconducting parallel-coupled microstrip lines. **IET Microwaves, Antennas & Propagation**, abr. 2014. v. 8, n. 6, p. 429–436.

[75] KUMAR, G. *et al.* Photoelectron spectroscopy of coordination compounds. II. Palladium complexes. **Inorganic Chemistry**, 1 fev. 1972. v. 11, n. 2, p. 296–300.

[76] ZOU, L. *et al.* In situ atomic-scale imaging of the metal/oxide interfacial transformation. **Nature Communications**, 21 ago. 2017. v. 8, n. 1, p. 307.

[77] ARAUJO, J. A. I. *et al.* Non-invasive antenna sensor for dielectric material identification at a distance. **Measurement**, jan. 2024. v. 224, p. 113842.

[78] ARTIGA, Xavier. Sidelobe Supression in Modulated Surface Reactance Antennas. [S.l.]: IEEE, 2018. p. 969–970.

[79] SOUZA, M. F. A. DE; SILVA, F. R. L. E; MELO, M. T. DE. A Novel LSB Discriminator for a 5-bit IFM Subsystem Based on Microstrip Band-Stop Filter. [S.l.]: IEEE, 2008. p. 36–39.